Topological stress triggers difficult-to-repair DNA lesions in ribosomal DNA with ensuing formation of PML-nucleolar compartment

Terezie Hornofova[1#], Alexandra Urbancokova[1#], Josef Novak[1], Sarka Salajkova[1$], Sona Stemberkova Hubackova[1$], Alena Uvizl[1$], Brian McStay[2], Zdenek Hodny[1*], Jiri Bartek[1,3,4*] and Pavla Vasicova[1*]

[1] Laboratory of Genome Integrity, Institute of Molecular Genetics of the Czech Academy of Sciences, Prague 142 20, Czech Republic

[2] Centre for Chromosome Biology, College of Science and Engineering, University of Galway, Galway, Ireland

[3] Genome Integrity Unit, Danish Cancer Society Research Center, Copenhagen, Denmark, Copenhagen DK-2100, Denmark

[4] Division of Genome Biology, Department of medical biochemistry and biophysics, Karolinska Institutet, Stockholm, Sweden

[$] Present address: **SSH**, Centre for Experimental Medicine, Institute for Clinical and Experimental Medicine, Prague 140 21, Czech Republic; **SS**, Department of Biochemistry, University of Zurich, 8057 Zurich, Switzerland; **AU**, DIANA Biotechnologies s.r.o., Vestec, Prague-West, Czech Republic

***** Correspondence to: **PV**, Ph.D.; Department of Genome Integrity, Institute of Molecular Genetics of the CAS, Videnska 1083, CZ 142 20 Prague 4, Czech Republic; Tel: (420)-24106 3151, Fax: (420)-24106 2289; E-mail: pavla.vasicova@img.cas.cz **ZH**, MD, Ph.D. E-mail: hodny@img.cas.cz and **JB**, MD, Ph.D.; E-mail: jb@cancer.dk

[#] equal contribution

ORCID

Terezie Hornofova https://orcid.org/0000-0002-6535-7989

Alexandra Urbancokova https://orcid.org/0009-0008-0741-1079

Josef Novak https://orcid.org/0000-0002-9764-6195

Sarka Salajkova https://orcid.org/0000-0002-1705-0755

Sona Stemberkova Hubackova https://orcid.org/0000-0002-3454-6840

Alena Uvizl https://orcid.org/0000-0002-5819-1482

Brian McStay https://orcid.org/0000-0002-5664-7781

Jiri Bartek http://orcid.org/0000-0003-2013-7525

Zdenek Hodny https://orcid.org/0000-0002-6454-6796

Pavla Vasicova https://orcid.org/0000-0002-9733-9929

Abstract

PML, a multifunctional protein, plays a crucial role in forming PML nuclear bodies, which are involved in various cellular processes, including stress responses. Under specific conditions, PML associates with nucleoli, forming PML nucleolar associations (PNAs). However, the stimuli leading to PNAs formation are unknown. Here we investigated these stimuli by exposure of cells to various genotoxic stresses. We reveal that the most potent inducers of PNAs share the ability to inhibit topoisomerases and RNA polymerase I. The inhibition of DNA double-strand break (DSB) repair augmented the occurrence of PNAs linking the stimulus for PNAs formation to unresolved DNA damage. The most potent treatment, doxorubicin, introduced DSBs into the rDNA locus. PNAs co-localized with damaged rDNA, sequestering it from active nucleoli. Using rDNA locus cleavage by I-PpoI, we proved that rDNA damage is a potent PNAs-inducing stimulus. Blocking homology-directed DSB repair (HDR), but not non-homologous end-joining (NHEJ) enhanced PNAs formation, identifying HDR as a PNAs modulator. Our findings have implications for genome stability and diverse diseases and indicate that PNAs form when difficult-to-repair rDNA DSBs occur in nucleoli, highlighting the interplay between the PML/PNAs and rDNA alteration caused by deficiencies in topoisomerases, inhibition of RNAPI, and rDNA DSBs destined for HDR.

Introduction

Promyelocytic leukemia protein (PML) was initially studied in the context of acute promyelocytic leukemia (APL), where specific chromosomal translocation t(15;17) occurs, resulting in the fusion of the PML gene with the retinoic acid receptor alpha (RARα) (1,2). The PML-RARα fusion protein is the primary oncogenic driver of APL (1). Subsequent investigations revealed that PML possesses diverse functions primarily associated with various stress response pathways. Notably, the complexity of PML's activities is evident in cancer biology, where it exhibits a dual role as both a tumor suppressor and a tumor promoter, depending on the cellular context and the specific signaling pathways involved (reviewed in (3)).

PML gene encodes seven splicing isoforms with shared N-terminus and variable C-termini, conferring the individual isoforms with different properties and functions (4-6). PML is essential for forming PML nuclear bodies (PML NBs), which serve as docking sites, facilitating mutual protein interactions and post-translational modifications (7). By this, PML affects diverse functions, including induction of cell cycle arrest, cellular senescence, apoptosis, participation in anti-viral responses, chromatin modification, transcriptional regulation, proteasomal degradation, and metabolic regulation (reviewed

in (8,9)). Two functions of PML are tightly linked to homology-directed DSB repair (HDR). First, PML-NBs house several HDR proteins, associate with persistent DNA damage foci, and PML depletion leads to decreased survival upon DNA damage requiring HDR-mediated repair (10-14). Second, PML is essential for forming APBs (alternative lengthening of telomeres-associated PML bodies), compartments in cells lacking telomerase, where telomeres are maintained via HDR-based mechanisms (15,16).

The nucleolus is the membrane-less organelle in the nucleus functionally dedicated to pre-rRNA synthesis and ribosome biogenesis (reviewed in (17)). In a human cell, there are approximately 300 copies of rDNA genes organized in tandem repeats, consisting of the 47S pre-rRNA (13 kb) and an intergenic spacer (30 kb) (18). The rDNA arrays are flanked by two mostly heterochromatic regions, a proximal junction on the centromeric side and a distal junction (DJ) on the telomeric side (19). Although these rDNA arrays are dispersed over the *p*-arms of five acrocentric chromosomes 13, 14, 15, 21, and 22 (20), they can form the innermost part of the same nucleolus (19). Notably, as active transcription of rDNA arrays triggers nucleolus formation, these regions are also called nucleolar organizing regions (NORs). It was reported that DJs presumably serve as NORs' anchors at the border of the nucleolus and fundamentally influence the nucleolar organization (19,21-23). The main threats of undermining rDNA integrity include: i) collisions between intensive pre-rRNA transcription and replication, inducing rDNA damage (24); ii) the intrinsic predisposition of rDNA repeats to recombination events that can occur in *cis* and cause gain or loss of rDNA units (25,26); and iii) the localization of several rDNA regions within the same nucleolus that under specific circumstances might induce interchromosomal entanglements and massive rearrangement (23). It is thought that both major DNA double-strand break (DSB) repair pathways, NHEJ and HDR, are involved in the repair of rDNA. The choice of the specific pathway depends on several factors and is still largely enigmatic. One of the hypotheses points out the importance of a damage threshold (reviewed in (27)). According to this notion, a low amount of uncomplicated DNA DSB generated, e.g., by homing endonucleases I-PpoI or AsiSI, can be repaired quickly by NHEJ inside the nucleolus without the concomitant RNAPI inhibition (28,29). In contrast, more complex and longer-persisting DNA DSBs trigger RNAPI inhibition followed by segregation of rDNA into nucleolar caps, where HDR is the main pathway involved (28,30).

Under certain stress conditions, PML can accumulate on the border of the nucleolar cap or form spherical structures containing nucleolar material next to the nucleolus, termed collectively PML nucleolar associations (PNAs). PNAs formation was observed in response to different types of genotoxic insults (31-34), upon proteasome inhibition (35), and in replicatively senescent hMSC and human fibroblasts (31,34). Doxorubicin, a topoisomerase inhibitor and one of the PNAs inducers, provokes a dynamic interaction of PML with the nucleolus, where the different phases linked to RNAPI inhibition can be discriminated into four basic structural subtypes of PNAs termed according to the 3D structures obtained by super-resolution microscopy as PML 'bowls', PML 'funnels', PML

'balloons' and PML nucleolus-derived structures (PML-NDS; (36)). The doxorubicin-induced inhibition of RNAPI leads to a nucleolar cap formation around which diffuse PML accumulates to form the PML bowl. Note that this event is rare as a minority of nucleolar caps are enveloped by PML (36). As the RNAPI inhibition continues, PML bowls protrude into PML funnels or transform into PML balloons wrapping the whole nucleolus. When the stress is relieved and RNAPI resumes activity, a PML funnel transforms into distinct compartments placed next to the non-segregated (i.e., reactivated) nucleoli, PML nucleolus-derived structures (PML-NDS). PML-NDSs contain nucleolar material, rDNA, and markers of DNA DSBs (36,37). Recently we unraveled that PML exon 8b and the SUMO-interacting motif (SIM) are the only domains responsible for the recognition of nucleolar cap and that this association is tightly regulated by $p14^{ARF}$-p53 and CK2 (37). Notably, exon 8b is unique for the PML IV isoform that plays the primary role in the clustering of damaged telomeres (16). Interestingly, PML determinants regulating the interaction with the nucleolus (nucleolar cap) are dispensable for the interaction of PML with persistent DNA DSBs after ionizing radiation (IR)(37), pointing again to the fine regulation of this interaction. Importantly, this specific interaction was observed after such diverse treatments as inhibition of the proteasome or exposure to doxorubicin and actinomycin D. Detailed knowledge about the molecular basis of signals inducing PNAs would help to understand this still enigmatic structure.

In this study, we investigated the nature of stimuli that signal the formation of PML-nucleolar associations. By analyzing factors involved in various cellular processes, such as inhibition of TOP2, TOP1, and RNAPI, replication stress, ionizing radiation, or proteasome inhibition, we defined features shared by stimuli leading to the formation of PNAs. In addition, as PNAs were found to associate with markers of DSB response, we examined how the cleavage of rDNA by endonuclease I-PpoI or modulation of DNA repair pathways affect the generation of PNAs. Based on our findings, we proposed that the induction of PML-nucleolar associations is primarily driven by topological stress and complex DNA damage, the repair of which relies on HDR.

Results

Simultaneous inhibition of topoisomerases and RNA polymerase I induces PML-nucleolar interaction.

To investigate the nature of signals triggering the formation of PNAs, we treated human telomerase-immortalized retinal pigment epithelial cells (RPE-1^{hTERT}) with a range of compounds affecting various cellular processes, including RNA polymerase I inhibitors, DNA topoisomerase I and II inhibitors, DNA-damaging agents, and compounds affecting pre-rRNA processing, etc. (see Supplementary Table 1). To identify features shared by the stimuli that trigger PML-nucleolar interactions, we quantified the number of nuclei with PML-nucleolar interactions (for overview of PNAs types, see Figure 1A) and followed several other parameters for each agent after 48-hour-long

exposure (see Figure 1B and Supplementary Figures 1A-E), such as the segregation of subunit of RNAPI PAF49 (as a readout of RNAPI inhibition), phosphorylation of serine 139 on histone H2AX (γH2AX foci, as a marker of DNA DSBs), stabilization of p53 protein levels (as an indicator of DNA damage response and cellular stress), and changes in levels of DNA topoisomerases I and II alpha (TOP1 and TOP2A).

Induction of replication stress by hydroxyurea and aphidicolin, inhibition of pre-rRNA processing by 5-FU (also referred to as antimetabolite), MG-132 (mainly used as proteasome inhibitor), and roscovitine (used as MAP-kinase inhibitor), generation of DNA damage by ionizing radiation (IR, 10 Gy) and thymidine analog bromodeoxyuridine (BrdU), and elevation of PML expression by IFNγ had little to no effect on triggering PNAs (<1% of cells; Figure 1B) indicating that stimuli leading to sole stabilization of p53 (Supplementary Figure 1C) or expression of PML are insufficient to signal for induction of these structures. Furthermore, none of these treatments caused segregation of PAF49, and if any PNAs were found, then only the PML-NDS (i.e., the specific variant of PNAs present next to the non-segregated nucleolus; see Figure 1A). In contrast, inhibitors of RNAPI and DNA topoisomerases were potent inducers of PNAs (Figure 1B). Further evaluation of the data demonstrated that the propensity for PNAs formation was highest (>5% of cells) for compounds that simultaneously inhibited RNAPI and downregulated TOP2A (Figure 1B, Supplementary Figures 1A and D). For instance, the TOP2 inhibitors doxorubicin and aclarubicin, and the TOP1 inhibitors camptothecin (CPT) and topotecan (TPT) inhibited RNAPI (as indicated by PAF49 segregation), induced the degradation of TOP2A, and generated PNAs in 22%, 12%, 17%, and 13% of cells, respectively. Notably, upon exposure to TOP1 inhibitors (CPT and TPT), only the highest tested concentration (50 µM) induced segregation of PAF49 and a high number of nuclei with PNAs (see Supplementary Figures 1F and G), indicating that the signal necessary for the emergence of PNAs is concentration dependent. The requirement for concurrent inhibition of RNAPI and TOP2A activity to achieve the highest number of PNAs was further highlighted by treatment with oxaliplatin and etoposide. Oxaliplatin, primarily reported as a DNA cross-linker, exhibited a combined effect on RNAPI inhibition and TOP2A downregulation, resulting in a high number of PNAs (12%). On the other hand, etoposide, a TOP2 poison, did not inhibit RNAPI even at a concentration of 50 µM (see Supplementary Figure 1F and G) and induced PNAs (predominantly in the form of PML-NDS) in less than 5% of cells (see Supplementary Figures 1F and G). We also tested three different inhibitors of RNAPI: actinomycin D (AMD), BMH-21, and CX-5461. All three inhibitors induced a decline of TOP2A but not TOP1 protein level. Notably, after prolonged, 2-day-long treatment, only BMH-21 and AMD robustly inhibited RNAPI, whereas CX-5461 did not. BMH-21 was one of the most potent inducers of PNAs, with 20% of cells with this structure present after treatment. In contrast, AMD and CX-5461 induced a comparable number of cells with PNAs (6% and 4%, respectively), ranking these treatments among weaker inducers of PNAs. Furthermore, despite the high number of cells with

PNAs in the population, BMH-21 and aclarubicin evoked a modest amount of γH2AX foci, indicating that the amount of DNA DSBs is not the primary factor signaling the formation of PNAs. In the same vein, IR, etoposide, and CX-5461 exposure induced high levels of γH2AX foci without concomitant occurrence of higher numbers of cells with PNAs, which in all cases, remained below the 5% of the cell population. These findings suggest that simultaneous impairment of TOP2A/topoisomerases and RNAPI activity enhance the signal for PML-nucleolus association. In contrast, the level of DNA DSBs does not correlate with the stimulation of the PML nucleolar interaction.

To investigate whether the signal for PNAs formation is directly linked to the abrogation of topoisomerase function and to exclude the possibility of non-specific effects of topoisomerase inhibitors, we downregulated TOP1, TOP2A, and TOP2B, respectively, by RNA interference. Downregulation of TOP1 or TOP2A, but not TOP2B (see Supplementary Figure 1H for knockdown efficiency; note two different siRNA targeting TOP2B were tested), induced the formation of PNAs (Figure 1C). Interestingly, in the first few days after the downregulation of TOP1, RNAPI remained active, and only PML-NDS were present (Figure 1C and Supplementary Figure 1I). However, at later time points (three and six days), RNAPI gradually became segregated and different types of PNAs, such as funnels and bowls, emerged (Supplementary Figure 1I). These results suggest that the signal for PNAs is directly linked to the loss of topoisomerase function, particularly TOP1 and TOP2A.

Based on the above findings, we proposed that PNAs generation is due to a change in DNA metabolism resulting from the combination of active pre-rRNA transcription and reduced topoisomerase activity. To test this hypothesis, we inhibited RNAPI activity using AMD or CX-5461 before adding doxorubicin or downregulating TOP1 (esiTOP1). The efficacy of RNAPI inhibition was confirmed by 5-FU incorporation (Supplementary Figure 1J and K). Surprisingly, in both cases, the cessation of pre-rRNA transcription before inhibition/downregulation of topoisomerases led to more PNAs than treatment with doxorubicin or TOP1 downregulation alone (Figure 1D). These results suggest that ongoing pre-rRNA transcription and subsequent treatment-induced collision are unnecessary to induce PNAs.

Overall, our data indicate that the defects in topoisomerase activity associated with the inhibition of RNAPI, but not collision with the ongoing rRNA transcription, represent the most potent signals for the association of PML with the nucleolus.

Induction of PNAs is augmented by the inhibition of specific DNA repair pathways

After analyzing these and our previous data (36,37), we argued that accumulated (r)DNA damage is responsible for prolonged RNAPI inhibition, leading to the association of PML with nucleoli. To verify this assumption, we examined whether modifying DNA repair pathways could impact the

development of PNAs caused by doxorubicin. First, we inhibited HDR in RPE-1^{hTERT} cells with B02, a compound that blocks RAD51 filament control of homologous strand displacement (inhibitor of RAD51; (38)). Initially, we applied a 0.75 µM concentration of doxorubicin, which generated the highest number of PNAs (Figure 1B), in combination with increasing doses of B02 (5, 10, and 20 µM; see Supplementary Figures 2A and B for the effect of B02 on RAD51 foci formation). Although the total number of PNAs was not significantly altered, we observed an increased proportion of balloon-like PNAs (Supplementary Figure 2C-E), which are predominantly associated with RNAPI inhibition (36). This indicates that inhibition of HDR shifted the dynamics of PNAs' progression toward early phases and that HDR is involved in DNA repair of doxorubicin-induced DNA damage. However, the combined treatment caused increased cell death, preventing further follow-up during recovery. Therefore, we also tested the combination of B02 with lower concentrations of doxorubicin (0.375 µM and 0.56 µM; Figure 2A-D). Co-treatment with 20 µM B02 for 48 hours significantly increased the number of cells with PNAs compared to doxorubicin alone (Figure 2A) and altered the proportion of specific PNAs subtypes (Figure 2B) toward the forms linked with RNAPI inhibition and nucleolar cap formation (36). These effects were concentration-dependent. While 0.375 µM doxorubicin alone induced predominantly formation of PML-NDS, adding 20 µM B02 resulted in a higher occurrence of bowl-, balloon-, and funnel-like PNAs. This shift to the presence of balloon-like PNAs linked with the disappearance of PML-NDS was even more augmented by the higher dose of doxorubicin (0.57 µM) combined with 20 µM B02. These findings indirectly suggest that doxorubicin exposure and inhibition of RAD51/HR caused, besides the elevated number of PNAs, the effective suppression of RNAPI activity.

Next, we analyzed the effect of HDR inhibition by B02 on the distribution of PNAs in the recovery phase, i.e., four days after doxorubicin removal when the last stage of PNAs, PML-NDS, prevails (Figure 2E-G). Adding 20 µM B02 to 0.56 µM and 0.375 µM doxorubicin significantly increased the number of PML-NDS (as shown in Figure 2E). This result indicates that inhibiting RAD51/HDR during doxorubicin treatment affects the dynamics of PNAs during the initial exposure period (two days) and during the recovery phase, likely due to defects in DNA break repair by HDR.

To investigate the contribution of NHEJ in the formation of doxorubicin-induced PNAs, we utilized a DNA PK inhibitor, Nu7441, to block the activity of DNA-dependent protein kinase (DNA PK), a kinase involved in NHEJ (39). The DNA PK inhibition with Nu7441 in combination with three concentrations of doxorubicin (0.375, 0.56, and 0.75 µM) did not significantly affect the proportion of nuclei with PNAs (Supplementary Figure 2F and G; for the effect of 1 µM Nu7441 on efficiency of DNA DSB repair see Supplementary Figures 1H and I), indicating that the inhibition of NHEJ is not associated with the formation of doxorubicin-induced PNAs.

The results obtained from the previous experiment indicated that doxorubicin-induced DNA damage is repaired preferentially by HR, and inhibition of this repair pathway positively affected PML nucleolar interaction. To investigate whether similar effects could be observed after DNA damage that utilizes different repair pathways, we selected etoposide. Repair of etoposide-induced DNA damage depends on TDP2, an enzyme that removes trapped topoisomerase II from the DNA end (40). To inhibit the repair, we downregulated TDP2 in RPE-1^{hTERT} cells after etoposide treatment by RNA interference (Supplementary Figure 2J) and analyzed PML distribution by indirect immunofluorescence. RNAPI was not inhibited, and only PML-NDSs were present in nuclei (Supplementary Figure 2K and L). However, the number of nuclei with PML-NDS significantly increased (Figure 2H), suggesting that persisting DNA damage can be the source of PNAs – PML-NDS.

Our findings suggest that inhibiting RAD51 during doxorubicin treatment or downregulating TDP2 during etoposide treatment induces a higher number of PNAs. Furthermore, since modulation of DNA repair affected PML nucleolar interaction, it can be assumed that the persistent (r)DNA damage generates a signal for PML interaction with the nucleolus.

Doxorubicin treatment induces PML wrapping around damaged rDNA loci and distal junctions of acrocentric chromosomes

It has been previously demonstrated that PNAs induced by doxorubicin co-localize with rDNA, rDNA-interacting proteins, and DNA damage markers (36,37). Since inhibiting DNA repair pathways after treatment with doxorubicin and etoposide altered PNAs formation, we hypothesized that the generation of PNAs is associated with direct damage to the rDNA locus rather than with general genomic DNA damage. To test this hypothesis, we conducted an immuno-FISH experiment to examine the co-localization of rDNA with a marker of DNA DSBs. Furthermore, to obtain a better understanding of the localization of rDNA loci in the chromosomal context and to discriminate individual nucleolar caps, we utilized besides rDNA probes also probes that hybridize with distal junction (DJ), a region situated on the telomeric end of the rDNA repeats and previously used as a marker of individual NORs (see the scheme in Figure 3A; (19)).

First, we examined the localization of rDNA, DJ, PML, and the nucleolar marker B23 in control cells two days after doxorubicin treatment and one day after doxorubicin removal. As shown in Supplementary Figure 3A for untreated cells, the rDNA signal was spread throughout the nucleolus, and the DJ signal was detected on the nucleolar rim as expected (19). After doxorubicin exposure, nucleolar caps emerged, and some of them were wrapped by PNAs (Supplementary Figure 3A). In several instances, a single PNA (funnel- or bowl-type) appeared to interact with several DJs – acrocentric chromosomes, bridging several nucleolar caps. Twenty-four hours after doxorubicin

removal, the PML-NDS emerged, and DJ or rDNA were observed inside or on the rim of these PNAs types (Supplementary Figure 3A). The co-localization between rDNA/DJ and PML in individual nucleoli was determined using the Fiji/Mosaic/Squassh plugin. Note that the co-localization analysis was also performed in the nucleoli in which PML was present only in the form of canonical PML-NBs (see the gallery of nucleoli in Supplementary Figure 3B). As manifested in Supplementary Figure 3C, we proved that both rDNA and DJ co-localized with PML in response to doxorubicin treatment. However, the co-localization coefficient was higher in nucleoli containing PNAs, indicating that the interaction between rDNA/DJ and PML is mainly realized in the form of PML nucleolar associations.

To demonstrate that doxorubicin induces damage in the form of DNA DSBs in rDNA/DJ, we performed immuno-FISH to detect the 53BP1 foci, a marker of DNA DSBs, together with PML, rDNA, and DJ in control cells and at three different time points after doxorubicin treatment (i.e., two days of doxorubicin exposure and 1- and 4-days after doxorubicin removal; Figure 3B). First, we performed a co-localization analysis for rDNA/DJ and PML to verify our previous findings on a different sample set. As shown in Figure 3C, we confirmed that doxorubicin treatment induced the co-localization between rDNA/DJ and PNAs. Notably, this co-localization was still detectable even four days after doxorubicin removal. We then used the same set of nucleoli to determine the extent of co-localizations between 53BP1 and rDNA/DJ. As shown in Figure 3D, we detected the presence of DNA DSBs in both the rDNA locus and DJ region. These findings indicate that the extent of co-localization decreased during the recovery phase. Furthermore, the analysis revealed that rDNA/DJ loci co-localized with 53BP1 even in nucleoli without the PNAs, although the size of co-localization in such nucleoli was lower. To investigate whether PNAs interact with the rDNA/DJ regions stained for DNA DSBs (53BP1 foci), we utilized the Squassh analysis to combine 53PB1-rDNA/DJ and PML-rDNA/DJ co-localization (for a detailed description, see Figure Legend and Methods). Figure 3E and Supplementary Figures 3D and E show an example of the segmentation, quantified overlay, and a 3D model of co-localization. Furthermore, an x/y-scatter plot is given to demonstrate the size of co-localization of rDNA(DJ) objects with 53BP1 foci (axis x) and PML (axis y). Using this approach, we found that about 71% of PNAs examined two days after doxorubicin treatment overlapped with rDNA or DJ-contained DNA DSBs marked by 53BP1 foci (Figure 3F).

To summarize, our data prove that doxorubicin induces DNA DSBs in the rDNA and DJ regions, which associate with PML, linking the rDNA damage in the short arm of acrocentric chromosomes with the induction of PML nucleolar association. Our data also imply that rDNA/DJ regions with DNA DSB/s are enveloped into PML-NDS after the reactivation of RNAPI and, by this mechanism, separated from the matter of active nucleolus.

Direct rDNA damage induced by endonuclease I-PpoI triggers the formation of PML-NDS

Our findings indicate that PML nucleolar associations are linked to rDNA damage. To validate this hypothesis, we used DNA homing-endonuclease I-PpoI to generate targeted breaks in rDNA, as the I-PpoI-induced cleavage site is located inside the rDNA locus in the 28S region (see the scheme in Figure 4A; (41,42)). To control the activity of I-PpoI, we generated RPE-1^{hTERT} single-cell clones with a regulatable expression of I-PpoI using the TRE3 GS promoter and destabilization domain FKBT (43). In all experiments, two clones (1A11 and 1H4) were used in which the I-PpoI was activated for 24 hours, and several parameters were followed at different time points (see experimental scheme in Figure 4B). As shown in Figure 4C and Supplementary Figures 4A and B, activating I-PpoI for 24 hours resulted in the appearance of 53BP1 and γH2AX foci on the border of the nucleolus, indicating the presence of (r)DNA breaks. To characterize the extent of (r)DNA damage and the dynamics of its repair, we quantified the number of 53BP1 foci at different time points using high-content microscopy. Nearly 90% of control cells showed no detectable (r)DNA damage, proving that DNA damage detected is linked explicitly to I-PpoI activity (Figure 4D). Twenty-four hours after I-PpoI expression, 53BP1 foci peaked and then gradually declined over the five-day recovery phase (Figure 4D). PML localized predominantly to regular PML-NBs, but PML structures containing nucleolar material marked by TOTO-3, resembling the PML-NDS, emerged in about 10% of the nuclei (Figure 4C and E and Supplementary Figure 4B). Strikingly, the PNAs specifically associated with nucleolar caps (i.e., bowl-, funnel-, and balloon-type) were absent, consistent with preserved RNAPI activity in most nucleoli (for FU incorporation assay, see Supplementary Figure 4C). Note that the DNA damage-associated 53BP1 foci associated with both canonical PML-NBs and PML-NDS, and not all PML-NDS-like structures co-localized or localized next to the 53BP1 signal (Supplementary Figure 4B and D). Next, we compared the PML-NDS-like structures induced by I-PpoI with those generated by doxorubicin by examining the accumulation of B23 and DHX9, which are distinct components of doxorubicin-induced PML-NDS (36). Although I-PpoI-induced PML-NDS contained B23 (see Figure 4F) with a level higher compared to the associated nucleolus (see Supplementary Figure 4E), the localization of DHX9 differed from that of doxorubicin-treated cells (Figure 4G and Supplementary Figure 4F and G), indicating similarities and differences in the composition of both structures. In control cells, DHX9 was homogenously distributed in the nucleoplasm. Two days after doxorubicin treatment, the DHX9 signal was excluded from the nucleolus, and during recovery, it relocalized into the nucleolus and accumulated in PML-NDS (Supplementary Figure 4F). In contrast to doxorubicin, two subpopulations of cells emerged after I-PpoI activation: one with DHX9 aggregates inside the nucleolus and the other with a similar distribution of DHX9 as in control cells (Figure 4G). The characteristic 'doxorubicin' pattern of DHX9 accumulation in PML-NDS was present only in a few I-PpoI-induced cells, mainly during the recovery phase (see a gallery of cells in Supplementary Figure 4G). Finally, we examined the

localization of RNAPI subunit PAF49 and UBF (activator of pre-rRNA transcription, often used as a marker of rDNA; (28,44)) in I-PpoI-activated cells. As illustrated in Figure 4H and I and Supplementary Figure 4H and I, the PML-NDS induced by I-PpoI were located adjacent to the nucleoli, where the UBF and PAF49 signals were detected in cavities distributed uniformly throughout the nucleolus and surrounded by the TOTO-3 signal. It should be noted that such a localization pattern of UBF and PAF49 indicates the presence of RNAPI activity (see control cells in Figures 4H and I). Notably, most of the PML-NDS contained the UBF signal, which was again localized in cavities surrounded by TOTO-3 (Figure 4H and Supplementary Figure 4H). Similarly, PAF49 showed comparable localization in PML-NDS (Figure 4I and Supplementary Figure 4I). Since both proteins are markers of rDNA localization, we infer that rDNA is present in at least some PML-NDS.

In conclusion, by utilizing a model of enzymatically induced rDNA breaks, we have demonstrated that the formation of the PML-nucleolar compartment is a direct consequence of rDNA damage. Furthermore, we have shown that the composition of this compartment is comparable to that seen in the more pleiotropic DNA damage induced by doxorubicin.

Inhibition of RAD51/HDR suppresses the formation of I-PpoI-induced PML-NDS

To investigate the effect of altered DNA repair on I-PpoI-induced PML nucleolar association, we activated I-PpoI and simultaneously applied a small-molecule inhibitor of RAD51 (B02) and DNA PK inhibitor (Nu7441), either separately or together, to inhibit HDR and/or NHEJ (Figure 5A). We then detected the extent of (r)DNA damage (number of 53BP1 foci) and the number of nuclei with PML-NDS using indirect immunofluorescence and high-content microscopy. These experiments were performed in two cell clones expressing I-PpoI, 1A11, and 1H4, 24 hours after I-PpoI activation and during the recovery phase (1, 2, and 5 days after medium exchange). As shown in whiskers plots and histograms in Figure 5B (clone 1A11) and Figure 5C (clone 1H4), inhibiting NHEJ with Nu7441 during I-PpoI activation significantly increased the number of (r)DNA damage foci at all time-points compared to the mock treatment. In contrast, inhibiting HR with B02 resulted in fewer 53BP1 foci than in control cells. Notably, simultaneous use of both drugs did not increase the number of 53BP1 foci compared to DNA PK inhibition alone; by contrast, the (r)DNA damage detected was significantly lower. These findings proved previous observations that NHEJ is the primary pathway involved in repairing I-PpoI-induced DSBs, and when HR is blocked, the I-PpoI-induced (r)DNA damage is repaired more efficiently (28).

Regarding the impact of DNA repair inhibition on I-PpoI-induced PNAs (PML-NDS) formation, we observed that inhibiting NHEJ with Nu7441 resulted in a higher number of cells with PML-NDS, which was consistent with a higher occurrence of DNA DSB. However, this trend was not statistically

significant (see Figure 5D and E). On the other hand, inhibiting HR with B02 significantly decreased the number of cells with PML-NDS in both clones 24 hours after treatment, in line with lowered DNA damage markers. During the recovery phase, the number of cells with PML-NDS after B02 treatment remained lower, and this decrease remained statistically significant at most time points. However, the simultaneous application of both inhibitors resulted in intriguing findings. Even though inhibiting both main repair pathways increased the (r)DNA damage (though not as extensively as observed in cells treated with Nu7441 only), the number of cells with PML-NDS was significantly lower 24 hours after I-PpoI activation compared to cells without application of inhibitors. Note that this significant difference balanced out during the recovery phase after the washout of the DNA repair pathway inhibitors. Moreover, five days after recovery from the I-PpoI insult, the number of cells with PML-NDS was comparable to the control population (I-PpoI only). These data suggest that adding B02 (blocking HR) inhibits the signal toward forming the PML-NDS.

Overall, inhibiting NHEJ after the I-PpoI insult did not significantly alter the number of cells with PML-NDS, despite the higher DNA damage, suggesting that NHEJ-associated rDNA repair is not linked to PNAs formation (i.e., the DNA DSBs suitable for NHEJ repair are not the primary source of PNAs). In contrast, inhibiting HDR/RAD51 during I-PpoI-induced rDNA damage, even in the presence of inhibited NHEJ, led to a decreased propensity for PML-NDS formation, indicating that intact HR is necessary for the generation of PNAs after I-PpoI.

In conclusion, our data strongly suggest that the association of PML with the nucleolus results from 1) difficult-to-repair rDNA damage and 2) topological aberrations in nucleolar caps/NORs. Importantly, this occurrence is altered by defects in HDR pathways as easy-to-repair DNA DSBs prone to repair by NHEJ do robustly induce the PNAs formation.

Discussion

Since 2001, the re-localization of PML upon various treatments into and next to the nucleolus was noticed. Still, the substantial signal inducing the PML nucleolar interaction has not been deciphered yet. This study shows that the essential feature of the most potent inducers of PNAs is the simultaneous inhibition of DNA topoisomerases (TOP2A or TOP1 with TOP2A) and RNAPI. Moreover, the downregulation of topoisomerases and the inhibition of RNAPI were accompanied by the generation of DNA DSBs in the rDNA/DJ locus associated with the nucleolus (NOR). Importantly, the rDNA/DJ locus (NOR) with DNA DSBs co-localized with PNAs not only upon RNAPI inhibition but also in PML-NDS after recovery of RNAPI activity, pointing to the putative sorting mechanism for damaged rDNA/DJ (NORs). This relationship between PNAs and damage of rDNA loci was supported by the observation that direct rDNA damage introduced by endonuclease I-PpoI provokes PML nucleolar interactions. Further, based on the notion that inhibiting specific DNA

repair pathways augments the PML nucleolar interaction, we assume that the underlying molecular mechanisms are linked to generating and processing a specific, difficult-to-repair type of rDNA alteration or damage.

PNAs result from genotoxic stress that relies on the deficiency of DNA topoisomerases and inhibition of RNAPI

The interaction of PML with the nucleolar surface was first described after exposure of mouse (MEF) and human fibroblasts (WI38) to doxorubicin, mitomycin C, and actinomycin D (32). The authors proposed that this interaction results from the specific type of genotoxic stress as ionizing radiation (IR) could not induce it. Later, Condemine *et al.* confirmed the targeting of PML to the nucleolus after genotoxic stress in human fibroblast MRC-5; however, they observed the re-localization of PML to nucleolus not only after doxorubicin and AMD but in contrast to the previous study (32), also after the IR (34). Here, we underpinned that this interaction results primarily from the genotoxic stress; however, the number and forms of these structures radically depend on the type of insults, supporting the hypothesis of Bernardi *et al.* that a particular type of genotoxic stress triggers the re-localization of PML to the nucleolar rim (32). By applying a broad panel of agents affecting diverse cellular processes, we found that the most potent inducers of PNAs, such as doxorubicin, inhibit two distinct processes: i) maintenance of DNA topology and ii) transcription of pre-rRNA. Although this notion might suggest that the signal to form the PML nucleolar compartment stems from conflicts between the ongoing pre-rRNA transcription and afflicted maintenance of DNA topology, it is inconsistent with other findings that the inhibition of RNAPI before depletion or inhibition of topoisomerases augmented the occurrence of PNAs. One possible explanation for these results is that topoisomerases participate in processes linked with RNAPI inhibition in the rDNA locus. For instance, inhibition of RNAPI could introduce topological aberrations of rDNA, the resolution of which depends on topoisomerase activity, and the unsolved topological challenges trigger the processes initiating the interaction of PML with nucleolus/nucleolar cap. The direct link between defects in the activity of topoisomerases and the interaction of PML with nucleolus was underscored by the observation that depletion of TOP1 and TOP2A (but not TOP2B) induced PNAs. Again, the inhibition of RNAPI before the downregulation of TOP1 augmented the formation of PNAs attesting to the concept that the deficiency of topoisomerase activity during pre-rRNA transcription is not the only stimulus to form PNAs and is consistent with implicates the hypothesis that specific topoisomerase activity is required to cope with the scenario of RNAPI inhibition. This concept is further supported by the observation that AMD, the potent antitumor antibiotic, which intercalates DNA preferentially at GC-rich regions (45), induced PNAs without the detectable DNA DSBs. Although AMD treatment caused degradation of TOP2A (but not TOP1), induced stabilization of p53, and segregation of PAF49 in all nucleoli (accounting for RNAPI inhibition), DNA DSBs were not detected. It should be emphasized that albeit nucleolar caps (the interface for PML nucleolar interaction) were established in all nuclei, the PNAs

were present only in a small fraction (6%) of nuclei, indicating that also another additional signal induced by a relatively rare event is involved in triggering PNAs formation. Given that the most potent inducers of PNAs are topoisomerase inhibitors, we presume that such signal relies on topological aberrations of DNA formed during the re-localization/wrapping/pulling of rDNA loci (NOR) into the nucleolar cap.

Unsolved topological aberrations in NOR/nucleolar cap result in PNAs formation

Generally, DNA topoisomerases are involved in the maintenance of DNA topology primarily during DNA replication and transcription (46) by their ability to introduce DNA single-strand breaks (TOP1) or DNA DSBs (TOP2) during their enzymatic cycle. The detailed analysis of the activity of individual topoisomerase types revealed their functional specificity (for a review, see, e.g., (47)). Nearly all PNAs-inducing treatments (except TOP1 downregulation) triggered the degradation of TOP2A. Additionally, the downregulation of TOP2A but not TOP2B provoked the formation of PNAs. Therefore, the stimulus for PNAs could arise from the deficiency in TOP2A activity. TOP2A generally acts during DNA replication and mitosis (48,49). Besides its ability to repair the aberrant supercoiling of DNA, it can potentially resolve DNA catenates and knots (reviewed in (47)). It is thought that TOP2A is essential for the termination of replication of highly repetitive sequences such as telomeres, centromeres, and rDNA (50). Danilovski *et al.* reported the role of TOP2A in the topological regulation of rDNA (51); they showed that the resolution of the human rDNA locus (sister chromatids) during mitosis depends on TOP2A. The fact that the degradation of TOP2A is a feature shared with all potent PNAs inducers raises the question of how the enzymatic activity of TOP2A is related to the PML nucleolar interaction. We propose that the excessive alteration of rDNA conformation during RNAPI inhibition and pulling of the repetitive rDNA region (NOR) from the nucleolar interior towards the nucleolar rim, when the nucleolar cap is forming, causes the topological changes (entanglements, catenates, and knots), in which resolution TOP2A participates. Although still unproven, the formation of rDNA entanglements/catenates/knots during nucleolar cap development was already mentioned in previous studies (19,23). Authors reported that during the pre-rRNA transcription, each NOR occupies its own territory, and when RNAPI is inhibited, each NOR is transformed into one nucleolar cap. Such strict territoriality can avoid the danger of inter-chromosomal interaction. Importantly, our results indicate that after treatment with doxorubicin, the most potent inducer of PNAs, the rule 'one NOR – one cap' was broken as several NORs met in one nucleolar cap and these caps were often wrapped by single PNA (e.g., Supplementary Figure 3A). Such a state indicates a higher probability of unwanted inter-chromosomal interactions associated with the formation of DNA catenates and knots which might be solved with difficulties without the activity of TOP2A. In this scenario, we propose that a lack of TOP2A activity results in initiating alternative processes involving PML nucleolar association.

Both tested TOP1 inhibitors (CPT, TPT) introduced DNA DSBs, caused inhibition of RNAPI, and degradation of TOP1 and TOP2A. Thus, the observed phenotype could result from defects in activities linked to both enzymes. Despite that, the downregulation of TOP1 by RNA interference induced PNAs without the substantial decline of TOP2A level; therefore, we consider that the decline of TOP1 enzymatic activity can contribute to the signal for PNAs formation. TOP1 removes negative and positive DNA supercoiling, which is introduced during the replication and transcription of DNA (52). Thus, the downregulation of TOP1 can produce an elevated amount of hyper-negatively or positively supercoiled DNA. The hyper-negatively supercoiled DNA forms alternative, non-B DNA, such as single-stranded DNA, G-quadruplexes, and right-handed (Z-form) DNA (53). In yeast, the single-strand DNA 'bubbles' were observed in transcribed rDNA region after downregulation of TOP1 (54). In several cancer cell lines, the downregulation of TOP1 affected the amount and distribution of R-loops (reviewed in (55)). Taken together, even a decline in enzymatic activity of TOP1 can induce the aberration(s) leading to PNAs formation.

TOP2 poisoning per se and the genesis of PNAs

As mentioned above, topoisomerase inhibitors are the most effective inducers of PNAs, except for etoposide. Even the highest etoposide concentration tested (50 µM, see Supplementary Figure 1F and G) cannot robustly inhibit RNAPI, despite the degradation of TOP2A was proved, and markers of DNA DSBs were present, indicating that the mechanism by which etoposide interferes with TOP2 activity is insufficient to signal PNAs formation. To better understand the respective mechanisms of toxicity of etoposide and doxorubicin (triggering PNAs in 5% and 22% of cells, respectively), we analyzed the critical differences. It is thought that etoposide acts as a pure TOP2 poison, stabilizing the TOP2-DNA covalent complexes (also referred to as ternary complexes) in a broad range of concentrations and, therefore, protecting the re-ligation of DNA (56). Thus, the formation of DNA DSBs is the final consequence of etoposide exposure. On the other hand, the anthracycline doxorubicin stabilizes the TOP2-DNA only at low concentrations, and the number of ternary complexes is always lower compared to etoposide (57). Besides the TOP2 poisoning activity, doxorubicin can inhibit TOP2-mediated decatenation (58,59), intercalates DNA, and by this alters DNA torsion and induces histone eviction (60), and elevates oxidative stress (61,62). Thus, the DNA damage introduced by doxorubicin is more complex than etoposide. Based on these findings, we hypothesize that the sole DNA DSBs introduced by freezing TOP2 in catalytic action do not cause sufficient aberration of (r)DNA to signal for extensive PML nucleolar interaction, despite the TOP2 activity being affected and DNA damage response being present. This observation implies that for the induction of PNAs, the introduced (r)DNA damage must be more complex and challenging to repair. Alternatively, the inflicted damage should primarily affect the topology of rDNA (NOR); thus, the deficiency of topoisomerases enhances the persistence of such damage.

Role of easy-to-repair (r)DNA DSBs in the genesis of PNAs

Our data show a complex relationship between the presence of DNA DSBs and stimuli triggering PNAs. After doxorubicin treatment, most PNAs contained rDNA with a marker of DNA DSBs, indicating a close link. The inhibition of the DNA DSBs repair pathway enhanced the number of cells with PNAs, and finally, DNA DSBs introduced directly into the rDNA locus by endonuclease I-PpoI triggered PML-NDS. Nevertheless, these data also imply that simple and probably easy-to-repair DNA DSBs, e.g., caused by I-PpoI or etoposide treatment, are not particularly potent inducers of PNAs. In concert, these treatments did not cause long-term RNAPI inhibition, leading to only a specific type of PNAs, PML-NDS. As mentioned, etoposide can trap TOP2 in the catalytic process. For successful DNA repair, the TOP2 adduct must be removed from the DNA ends by the enzyme TDP2 (40,63), then the remaining DNA DSBs with 4-base cohesive overhang are resolved by NHEJ (64,65). Likewise, the endonuclease I-PpoI cleaves the DNA forming a 4-base cohesive overhang, and such DNA DSBs are mostly repaired by NHEJ (28,66). Moreover, the HDR repair after such damage in repetitive rDNA locus is paradoxically error-prone because it leads to the loss of rDNA repeats (28). We observed that the inhibition of NHEJ upon I-PpoI attack could restrict DNA repair as the level of DNA DSBs was elevated compared to the control mock conditions. On the other hand, the elevated amount of such DNA DSBs did not cause a significant increase in the number of PNAs (see Figure 5B-E). These results indicate that even the persistent DNA DSBs targeted for repair by NHEJ are not sufficient to signal for PNAs formation, and some other events should be considered to support this process. Importantly, we observed that upon I-PpoI cleavage, the inhibition of HDR lowered the amount of both DNA DSBs and PNAs, relating the PNAs formation directly to the presence of DNA DSBs. However, when we restricted both repair pathways, NHEJ and HDR, simultaneously during the I-PpoI activation, the number of DNA DSBs was lower compared to NHEJ alone but still higher than in the circumstances of the unlimited DNA repair. These conditions were not associated with the formation of PNAs, as their number was significantly lower compared to I-PpoI restriction alone. This result challenges a positive correlation between the number of DNA DSBs and PNAs. More likely, it indicates that the recombination step after the I-PpoI insult is the primary source of PNAs. However, another controversy must be explained in the face of this interpretation. The inhibition of RAD51-dependent invasion of DNA filament during the doxorubicin treatment had the opposite effect, as the number of nuclei with PNAs was elevated, indicating that the defect in HR-directed repair boosted the PNAs formation. This apparent discrepancy can be explained by a different type of DNA damage present. As mentioned before, doxorubicin induces not only simple DNA DSBs but also complex DNA lesions. It was described that DNA repair is prolonged after doxorubicin treatment compared to etoposide (60). It was additionally shown that DNA repair after doxorubicin treatment relies less on NHEJ compared to etoposide (67). The direct involvement of RAD51 (and HDR) in the repair of DNA damage induced by doxorubicin was observed in multiple

myeloma cells and HCT-116 colon carcinoma cells as in both cases, the combination of B02 with doxorubicin induces elevated amount of DNA DSBs and apoptosis (68,69). These observations support our notion that inhibition of HDR after doxorubicin treatment produces irreparable DNA damage (probably not simple DNA DSBs), which can negatively affect the RNAPI activity resulting in the formation of the nucleolar cap, which can contain not only the topological aberrations requiring TOP2 activity but also difficult-to-repair DNA DSBs. Off note, our hypotheses that DNA DSBs prone to repair by NHEJ are not the dominant signal for PNAs is supported by the observation that repair of DNA damage induced by TOP1 inhibitors such as CPT (one of the most potent inducers of PNAs) is not dependent on NHEJ (67). To summarize, although we found that endonuclease I-PpoI, which produces DNA DSBs directed for NHEJ repair, can trigger the process leading to the formation of a specific PNAs form (PML-NDS), other findings indicate that an additional event following DNA aberration/s must occur to induce the PML nucleolar interaction. Moreover, our observations indicate that HDR, rather than NHEJ, participates in signaling that induces PNAs formation.

The analogy between PNAs and PML cages formed during herpesvirus infection

In the previous part of the Discussion, we discussed the topological aberrations and DNA DSBs as possible signals for forming PNAs. Nevertheless, we cannot exclude that the fragments (circles) of (r)DNA that can be formed during the HDR between the individual repeats in repetitive regions can contribute to signal triggering the PNAs. Such a consequence of recombination, albeit in the telomeric repetitive DNA region, was detected during the ALT (16). We suppose that the loss of rDNA copies observed by Warmerdam *et al.* during the repair of I-PpoI-induced DNA DSBs by HDR is also accompanied by the presence of rDNA fragments or circles (28). Moreover, as the inhibition of HDR upon I-PpoI insult attenuated the number of PNAs, we believe that such a product of HDR could indeed trigger PNAs. The affinity of PML to linear/circular DNA pieces can be adopted from its role in antiviral defense. It is known that PML forms PML-NBs around various viral genomes, thus controlling their replication (for a review, see (70)). This observation was extended by Reichelt *et al.* showing that the human alpha herpesvirus Varicella zoster virus induces the formation of the PML cages that contain viral nucleocapsids and, by their shape and size, resemble PML-NDSs (71). The analogy with PNAs (PML-NDS) is supported by the observation that this phenomenon depends, similarly to PNAs, on the PML IV isoform and its exon8 (71). Additionally, it was recently published that a mutated form of hCMV defective in disruption of PML-NBs also induced PML cages enveloping the sole viral genome together with nucleocapsids (72). These results indicate that the incoming viral DNA initiates the interaction with PML-NBs and, under certain circumstances, triggers the genesis of giant PML-NBs (PML cages) that imprison the viral genome and newly formed nucleocapsids. Notably, the formation of hCMV-induced PML cages is driven by interferons and ATM/p53, indicating the involvement of DNA damage response in this event.

Conclusion

By examining a set of genotoxic and other treatments, we discovered that PML nucleolar associations are triggered by the complex and difficult-to-repair lesions in nucleolar rDNA (NORs) resulting from topological stress and inhibition of rDNA transcription. Although we did not define the exact type(s) of rDNA locus aberration, we assume that variety (probably more than one) DNA alterations, such as DNA catenates, knots or circles, inter- or intra-chromosomal entanglements, including those dependent on homology-directed repair (e.g., HDR-prone DNA DSBs) induce signals leading to generation of PNAs. The molecular role of PNAs in processing these rDNA impairments is unknown and should be further examined. Nevertheless, we can at least suppose that PNAs can recognize damaged DNA and, by developing PML-NDS next to the active nucleolus, segregate aberrant rDNA from undamaged NORs. Identifying groups of chemotherapeutic drugs that can introduce difficult-to-repair damage into the rDNA locus (NORs) and induce long-term RNAPI inhibition sensitizing cells to cell death can be explored to investigate synergic effects of new combinations of topoisomerase and RNA polymerase I inhibitors, particularly in the context of cancer therapy.

Material and Methods

Chemicals and antibodies

4',6-diamidino-2-phenylindole (DAPI; D9542), aphidicolin (A0781), actinomycin D (50-76-0), 5-bromo-2´-deoxyuridine (B5002), BMH-21 (SML1183), camptothecin (C9911), CX-5461 (1138549-36-6), DIG-Nick Translation Mix (11745816910), doxorubicin hydrochloride (D1515), doxycycline hyclate (D9891), etoposide (E1383), 5-fluorouracil (F6627), 5-fluorouridine (F5130), G418 disulfate salt (G5013), hydroxyurea (H8627), MG-132 (C2211), oxaliplatin (O9512), RAD51 Inhibitor B02 (SML0364), roscovitine (R7772) and topotecan hydrochloride (T2705) were all purchased from Sigma-Aldrich/Merck (Darmstadt, Germany). Aclarubicin (A2601) was obtained from APExBIO (Houston, TX, USA), pyridostatin (4763) from TOCRIS (Bristol, United Kingdom), and the interferon gamma recombinant protein (300-02) from Peprotech (Rocky Hill, NJ, USA), TOTO-3 (T-3604). Lipofectamine RNAiMAX Reagent (13778075) and ProLong™ Gold Antifade Mountant (P36934) were obtained from Thermo Fisher Scientific (Waltham, MA, USA), NU 7447 (3712) was from BioTechne/NovusBiological (Minneapolis, USA), Shield-1 (AOB1848) from AOBIOUS (Gloucester, MA, USA). Nick translation DNA labeling system 2.0 (ENZ-GEN111-0050), and Red 650 [Cyanine-5E] dUTP (ENZ-42522) from Enzo Biochem (New York, NY, USA), Hybrisol VII (ICNA11RIST139010) from VWR International (Singapore).

Specification of primary and secondary antibodies used throughout the study is listed in Supplementary Table 2.

Cell culture

Immortalized human retinal pigment epithelial cells (RPE-1^{hTERT}, ATCC) were cultured in Dulbecco's modified Eagle's medium (Gibco/Thermo Fisher Scientific, Waltham, MA, USA) containing 4.5 g/L glucose and supplemented with 10% fetal bovine serum (Gibco/Thermo Fisher Scientific, Waltham, MA, USA) and antibiotics (100 U/mL penicillin and 100 µg/mL streptomycin sulfate, Sigma, St. Louis, MO, USA). The cells were cultured in normal atmospheric air containing 5% CO_2 in a standard humidified incubator at 37°C on a tissue culture dish (TPP Techno Plastic Products AG, Trasadingen, Switzerland). For treatments, see Supplementary Table 1. For IR exposure, the cells were irradiated with orthovoltage X-ray instrument T-200 (Wolf-Medizintechnik) using a dose of 10 Gy. The cells with inducible expression of endonuclease I-PpoI were derived from RPE-1^{hTERT} (the detailed protocol of their generation follows). The culture conditions were the same as for RPE-1^{hTERT}, except the certified TET-free 10% fetal bovine serum (Gibco/Thermo Fisher Scientific, Waltham, MA, USA) was used to repress the expression of I-PpoI. The seeding concentration for all experiments was 20,000 cells/cm^2. The 0.5 µM Shield-1 and 1 µM doxycycline were used to induce I-PpoI. The 10 µM B02 and 1 µM Nu7441 were added simultaneously with doxorubicin or Shield and doxycycline to inhibit HR or NHEJ, respectively.

Generation of cell lines with inducible expression of I-PpoI

All plasmids and primers used in this study are listed in Supplementary Table 3 and Supplementary Table 4, respectively. To generate a cell line with the regulatable expression of endonuclease I-Ppo-I, the lentiviral plasmid pLVX-TetOne-neo bearing a cassette with endonuclease I-PpoI fused to destabilization domain FKBP and HA-tag (pLVX-TETOne-neo-FKBP-PPO-HA) was prepared as follows. For all DNA amplification steps, Phusion High-Fidelity DNA Polymerase (M0530L) was used. DNA fragment with FKBP-I-Ppo-I-HA was amplified from plasmid pCDNA4TO-FKBP-PPO-HA (73) using primers GA-PpoI-LVXpur-fr-F and GA-PpoI-LVXpur-fr-R and then, using Gibson assembly, was inserted into pLVX-TETOne-neo plasmid cleaved by BamHI, EcoRI and dephosphorylated by Shrimp Alkaline Phosphatase (EF0511, Fermentas). The correct fusion was verified by sequencing. The plasmid pLVX-TET-ONE-neo was prepared by exchange of region coding for puromycin N-acetyltransferase (*puromycin resistance)* with DNA fragment coding for neomycin phosphotransferase (*npt; Neomycin resistance*). First, the core of pLVX-TETOne-Puro was linearized by PCR using primers GA-V-LVXpuro-F and GA-V-LVXpuro-R, and the DNA fragment with *npt* gene was obtained by PCR amplification of plasmid pCDH-CMV-MCS-EF1-Neo using primers GA-F-neo-R and GA-F-neo-F. Finally, both fragments were assembled by Gibson assembly, and the correct fusion was verified by sequencing. The stable RPE-1^{hTERT} cells with doxycycline-

inducible expression of FKBP-PpoI-HA were generated by lentiviral infection and subsequent selection with G418 (1.12 mg/mL). Afterward, the resistant cells were seeded into the 96-well plate to isolate single-cell clones. The generated cell lines were inspected for mycoplasma contamination and then for expression of I-PpoI.

Indirect immunofluorescence, high-content, and confocal microscopy

Cells grown on glass coverslips were fixed with 4% formaldehyde in PBS for 15 min, permeabilized in 0.2% Triton X-100 in PBS for 10 min, blocked in 10% FBS in PBS for 30 min, and incubated with primary antibodies for 1 hour, all in RT. After that, cells were washed thrice in PBS for 5 min, and secondary antibodies were applied in RT for 1 hour. For some experiments, 1 μM TOTO-3 was applied together with secondary antibodies. Subsequently, cells were counterstained with 1 μg/mL DAPI for 2 min, washed thrice with PBS for 5 min, and let dry. After that, coverslips were mounted in Prolong Gold Antifade mountant. The wide-field images were acquired on the Leica DM6000 fluorescent microscope using the HCX PL APO 63×/1.40 OIL PH3 CS and HCX PL APO 40×/0.75 DRY PH2 objectives and monochrome CCD camera Leica DFC 350FX (Leica Microsystems GmbH, Wetzlar, Germany); or on the Nikon Eclipse Ti2 Inverted Microscope with CFI PL APO 60×/1.40 OIL PH3 objective and DS-Qi2 high-sensitivity monochrome camera Andor Zyla VSC-07008. High-content image acquisition was made on the Olympus IX81 microscope (Olympus Corporation, Tokyo, Japan) equipped with ScanR module using the UPLFN 40× /1.3 OIL objective and sCMOS camera Hamamatsu ORCA-Flash4.0 V2 (Hamamatsu Photonics, Shizuoka, Japan). The data were analyzed using ScanR Analysis software (Olympus Corporation, Tokyo, Japan). High-resolution images were captured by a confocal Leica STELLARIS 8 microscope equipped with HC PL APO 63×/1.40 OIL objective using type F immersion oil (Leica, 11513859), DAPI was excited by 405 nm laser, whereas Alexa Fluor® 488, Alexa Fluor® 568 and TOTO-3 were excited by a white light laser tuned to 499 nm, 579 and 642 nm, respectively, and the signal was bidirectionally sequentially scanned with the use of hybrid detectors. Images were acquired as a sufficient number of Z-stacks with 0.2 μm step to cover the whole nuclei. The images were acquired and processed with Leica LIGHTNING deconvolution set to maximal resolution, but with the pinhole open to 1 AU and Zoom set to 8, large nuclei were rotated diagonally. The images obtained by immune-FISH and used for the analysis of the link between rDNA/DJ DNA locus and PML and DNA damage were captured by confocal laser scanning inverted microscope DMi8 with confocal head Leica TCS SP8 and equipped by HC PL APO 63×/1.40 OIL CS2; FWD 0.14; CG 0.17 | BF, POL, DIC objective using type F immersion oil (Leica, 11513859). The Alexa Fluor® 408 was excited by UV laser (405 nm), whereas Alexa Fluor® 488, rhodamine, and enhanced Cyanine 5-dUTP were excited by a white light laser tuned to 499 nm, 552 and 638 nm, respectively. The signal was bidirectionally sequentially scanned, and images were acquired as a sufficient number of Z-stacks with 0.2 μm step to cover whole nuclei. The obtained images were deconvoluted using Huygens Professional 20.10 software. All images were processed

using Fiji/ImageJ2 software (74,75). For co-localization analysis, the Fiji plugin Mosaic/Squassh (Squassh – segmentation and quantification of subcellular shapes) was used. The software was used according to the protocol and guidelines recommended by the authors (76). To prepare 3D co-localization models, a co-localization mask was generated as an overlap of individual masks generated by Squassh. Co-localization mask and the masks of individual channels were then upscaled by factor 10, and their surfaces were visualized in Imaris software (Oxford Instruments).

rDNA immuno-FISH

For immuno-FISH, the procedure described previously was used (44). Briefly, RPE-1^{hTERT} cells were grown on Superfrost Plus slides (R886761, P-lab), washed with PBS, fixed with 4% formaldehyde at RT for 10 min, and washed 3× 10 min with PBS. After that, the cells were permeabilized with 0.5% Triton X-100/PBS for 10 min at RT, washed 3× 10 min with PBS, and incubated for 2 hours in 20% glycerol/PBS. The slides were then snap-frozen in liquid nitrogen and stored at -80 °C. To produce fluorescent FISH probes, plasmid (for rDNA probe, Supplementary Table 3) or BAC (for DJ probe, Supplementary Table 3) DNA was labeled by nick-translation according to the manufacturer's instructions. The rDNA probe binds a 12-kb segment of rDNA intergenic spacer (immediately upstream of the promoter), while the DJ probe covers the interval between 76.5 kb and 259.4 kb distal to rDNA. For labeling, the slides were rinsed with PBS for 3× 10 min, washed briefly with 0.1 M HCl, incubated in 0.1 N HCl for 5 min, washed in 2× SSC (30 mM sodium citrate, 300 mM sodium chloride, pH 7) for 5 min, and let dry. The slides were then incubated with equilibration buffer (50% formamide/2× SSC) for 15 min at 37 °C. After 15 min, a DNA probe in Hybrisol VII was applied to clean coverslips, the equilibration buffer was shaken off the slides with cells, and the slides were lowered on the coverslips with the probe. The slides were then sealed, denatured for 12 min at 73 °C on a heating block, and incubated at 37°C for 16 – 48 h. After that, the coverslips were removed, and the slides were washed 3× 5 min with 50% formamide/2× SSC at 42°C; and 3× 5 min with 0.1× SSC preheated to 60°C. Then, the slides were washed 3× 5 min with PBS and immunofluorescence staining, and microscope imaging was performed as described above.

5-FU incorporation assay

For the 5-FU incorporation assay, cells were incubated with 1 mM 5-FU for 30 min at indicated time points after doxorubicin treatment and removal. After that, cells were fixed with 4% formaldehyde at RT for 15 min, and the 5-FU incorporation was visualized using anti-BrdU antibody cross-reacting with 5-FU. The standard protocol for immunofluorescence described above was used.

RNA interference

The cells were plated on 6-well plates one day before esi/siRNA transfection. esiRNAs targeting topoisomerase 1 (EHU101551) and topoisomerase 2α (EHU073241) were purchased from Sigma-Aldrich/Merck (Darmstadt, Germany) and transfected into cells in a final amount of 300 ng. siRNA targeting topoisomerase 2beta (5'CGAUUAAGUUAUUACGGUUtt 3', s106; 5' GAGUGUACACUGAUAUUAAtt 3', s108; both purchased at Ambion/ThermoFIsher Scientific), TDP2 (5' GUGGUGCAGUUCAAGAUCAtt 3'; obtained from Sigma-Aldrich/Merck) and non-targeting siRNA (Silencer® Select Negative Control No. 1, 4390843; Ambion/ThermoFIsher Scientific)) were transfected into cells at a final amount of 30 pM. The transfections were performed using Lipofectamine™ RNAiMAX, according to the manufacturer's instructions.

SDS-PAGE and immunoblotting

Cells were harvested into SDS sample lysis buffer (62.5 mM Tris-HCl, pH 6.8, 2% SDS, 10% glycerol), boiled at 95°C for 5 min, sonicated and centrifuged at 18,000×g for 10 min. The concentration of proteins was estimated by the BCA method (Pierce Biotechnology Inc., Rockford, USA). Equal amounts of total protein were mixed with DTT and bromphenol blue to final concentration of 100 mM and 0.01%, respectively, and separated by SDS-PAGE (8%, 12%, or 4 – 12% gradient polyacrylamide gels were used). The proteins were electrotransferred to a nitrocellulose membrane using wet or semi-dry transfer. Immunostaining followed by ECL detection was performed. The intensity of the bands was measured in Fiji/ImageJ Gel Analyzer plugin, and the protein levels were calculated as the band intensities of the proteins of interest, related to the band intensities of loading control, while the relative intensity of untreated cells (or cells treated with a dissolvent – acetic acid or DMSO) was set as one.

Abbreviations

53BP1, p53,binding protein 1; **5-FU**, 5-fluorouracil; **ALT**, alternative lengthening of telomeres; **AMD**, actinomycin D; **APB**, ALT-associated PML-NBs; **APL**, acute promyelocytic leukemia; **BrdU**, bromodeoxyuridine; **CPT**, camptothecin; **CK2**, casein kinase 2; **DNA PK**, DNA-dependent protein kinase; **DSB**, double-strand break; **hCMV**, human cytomegalovirus; **HDR**, homologous recombination-directed repair; **hMSC**, human mesenchymal stem cells; **HR**, homologous recombination; **HU**, hydroxyurea; **IFNγ**, interferon gamma; **immuno-FISH**, immunofluorescence-in situ hybridization; **IR**, ionizing radiation; **NC**, non-targeting control; **NHEJ**, non-homologous end joining; **NOR**, nucleolar organizing region; **PML**, promyelocytic leukemia protein; **PML-NBs**, promyelocytic leukemia nuclear bodies; **PML-NDS**, PML nucleolus-derived structure; **PNAs**, PML-

nucleolar associations; **pre-rRNA**, precursor ribosomal RNA; **RARα**, retinoic acid receptor alpha; **rDNA**, ribosomal DNA; **RNAi**, RNA interference; **RNAPI**, RNA polymerase I; **RPE-1^{hTERT}**, telomerase-immortalized human retinal pigment epithelial cells; **SIM**, SUMO-interacting motif; **siRNA**, small interfering RNA; **TDP2**, tyrosyl-DNA phosphodiesterase 2; **TOP1**, topoisomerase 1; **TOP2**, topoisomerase 2; **TPT**, topotecan; **UBF**, upstream binding factor; **γH2AX**, histone H2AX phosphorylated on serine 139.

Authorship contribution statement

TH and AU conceptualized, designed and performed the experiments of the project, conceptualized, designed, and performed the experiments of the project. PV conceptualized, designed, and performed the experiments and wrote the original draft; JN, SS, SS-H, and AU performed the experiments; BMS contributed to the finalization of the draft; JB and ZH conceptualized the experiments and contributed to the writing and finalization of the draft.

Acknowledgments

This study was supported by Grant Agency of the Czech Republic (Project 19-21325S), and Institutional Grant (Project RVO 68378050). ZH and PV were supported in part by the project National Institute for Cancer Research (Programme EXCELES, ID Project No. LX22NPO5102) – Funded by the European Union – Next Generation EU. JB was supported in part by the Danish Cancer Society grant (R322-A17482), The Danish Council for Independent Research grant (1026-00241B), and the Novo Nordisk Foundation grant (NNF20OC0060590). We acknowledge the Light Microscopy Core Facility, IMG, Prague, Czech Republic, supported by grants "National Infrastructure for Biological and Medical Imaging" (MEYS – LM2023050), "Modernization of the national infrastructure for biological and medical imaging Czech-BioImaging" (MEYS – CZ.02.1.01/0.0/0.0/18_046/0016045) and formal National Program of Sustainability NPUI LO1220 and LO1419 (RVO: 68378050-KAV-NPUI), for their support with the confocal, widefield imaging, and image analysis presented herein. We would like to thank Marketa Vancurova, Martin Capek, Ivan Novotny, Helena Chmelova, and Jiri Cerny for their excellent technical support.

Conflict of interest

We confirm that the data presented in the manuscript are novel, they have not been published and are not under consideration for publication elsewhere. The authors declare they have no conflict of interest.

References

1. de Thé, H., Chomienne, C., Lanotte, M., Degos, L. and Dejean, A. (1990) The t(15;17) translocation of acute promyelocytic leukaemia fuses the retinoic acid receptor alpha gene to a novel transcribed locus. *Nature*, **347**, 558-561.
2. Borrow, J., Goddard, A.D., Sheer, D. and Solomon, E. (1990) Molecular analysis of acute promyelocytic leukemia breakpoint cluster region on chromosome 17. *Science*, **249**, 1577-1580.
3. Datta, N., Chakraborty, S., Basu, M. and Ghosh, M.K. (2020) Tumor Suppressors Having Oncogenic Functions: The Double Agents. *Cells*, **10**, 46.
4. Bernardi, R. and Pandolfi, P.P. (2007) Structure, dynamics and functions of promyelocytic leukaemia nuclear bodies. *Nat Rev Mol Cell Biol*, **8**, 1006-1016.
5. Nisole, S., Maroui, M.A., Mascle, X.H., Aubry, M. and Chelbi-Alix, M.K. (2013) Differential Roles of PML Isoforms. *Front Oncol*, **3**, 125.
6. Jensen, K., Shiels, C. and Freemont, P.S. (2001) PML protein isoforms and the RBCC/TRIM motif. *Oncogene*, **20**, 7223-7233.
7. Van Damme, E., Laukens, K., Dang, T.H. and Van Ostade, X. (2010) A manually curated network of the PML nuclear body interactome reveals an important role for PML-NBs in SUMOylation dynamics. *Int J Biol Sci*, **6**, 51-67.
8. Guan, D. and Kao, H.Y. (2015) The function, regulation and therapeutic implications of the tumor suppressor protein, PML. *Cell & bioscience*, **5**, 60.
9. Corpet, A., Kleijwegt, C., Roubille, S., Juillard, F., Jacquet, K., Texier, P. and Lomonte, P. (2020) PML nuclear bodies and chromatin dynamics: catch me if you can! *Nucleic Acids Res*, **48**, 11890-11912.
10. Vancurova, M., Hanzlikova, H., Knoblochova, L., Kosla, J., Majera, D., Mistrik, M., Burdova, K., Hodny, Z. and Bartek, J. (2019) PML nuclear bodies are recruited to persistent DNA damage lesions in an RNF168-53BP1 dependent manner and contribute to DNA repair. *DNA Repair (Amst)*, **78**, 114-127.
11. Attwood, K.M., Salsman, J., Chung, D., Mathavarajah, S., Van Iderstine, C. and Dellaire, G. (2020) PML isoform expression and DNA break location relative to PML nuclear bodies impacts the efficiency of homologous recombination. *Biochemistry and cell biology = Biochimie et biologie cellulaire*, **98**, 314-326.
12. Boichuk, S., Hu, L., Makielski, K., Pandolfi, P.P. and Gjoerup, O.V. (2011) Functional connection between Rad51 and PML in homology-directed repair. *PLoS One*, **6**, e25814.
13. Yeung, P.L., Denissova, N.G., Nasello, C., Hakhverdyan, Z., Chen, J.D. and Brenneman, M.A. (2012) Promyelocytic leukemia nuclear bodies support a late step in DNA double-strand break repair by homologous recombination. *J Cell Biochem*, **113**, 1787-1799.
14. Munch, S., Weidtkamp-Peters, S., Klement, K., Grigaravicius, P., Monajembashi, S., Salomoni, P., Pandolfi, P.P., Weisshart, K. and Hemmerich, P. (2014) The tumor suppressor PML specifically accumulates at RPA/Rad51-containing DNA damage repair foci but is nonessential for DNA damage-induced fibroblast senescence. *Mol Cell Biol*, **34**, 1733-1746.
15. Yeager, T.R., Neumann, A.A., Englezou, A., Huschtscha, L.I., Noble, J.R. and Reddel, R.R. (1999) Telomerase-negative immortalized human cells contain a novel type of promyelocytic leukemia (PML) body. *Cancer Res*, **59**, 4175-4179.
16. Zhang, J.M., Genois, M.M., Ouyang, J., Lan, L. and Zou, L. (2021) Alternative lengthening of telomeres is a self-perpetuating process in ALT-associated PML bodies. *Mol Cell*, **81**, 1027-1042 e1024.
17. Pederson, T. (2011) The nucleolus. *Cold Spring Harb Perspect Biol*, **3**, a000638.
18. Gonzalez, I.L. and Sylvester, J.E. (1995) Complete sequence of the 43-kb human ribosomal DNA repeat: analysis of the intergenic spacer. *Genomics*, **27**, 320-328.

19. Floutsakou, I., Agrawal, S., Nguyen, T.T., Seoighe, C., Ganley, A.R. and McStay, B. (2013) The shared genomic architecture of human nucleolar organizer regions. *Genome Res*, **23**, 2003-2012.
20. Henderson, A.S., Warburton, D. and Atwood, K.C. (1972) Location of ribosomal DNA in the human chromosome complement. *Proc Natl Acad Sci U S A*, **69**, 3394-3398.
21. van Sluis, M., van Vuuren, C., Mangan, H. and McStay, B. (2020) NORs on human acrocentric chromosome p-arms are active by default and can associate with nucleoli independently of rDNA. *Proc Natl Acad Sci U S A*, **117**, 10368-10377.
22. van Sluis, M., Gailin, M.O., McCarter, J.G.W., Mangan, H., Grob, A. and McStay, B. (2019) Human NORs, comprising rDNA arrays and functionally conserved distal elements, are located within dynamic chromosomal regions. *Genes Dev*, **33**, 1688-1701.
23. Mangan, H. and McStay, B. (2021) Human nucleoli comprise multiple constrained territories, tethered to individual chromosomes. *Genes Dev*, **35**, 483-488.
24. Lin, Y.L. and Pasero, P. (2012) Interference between DNA replication and transcription as a cause of genomic instability. *Current genomics*, **13**, 65-73.
25. Stankiewicz, P. and Lupski, J.R. (2002) Genome architecture, rearrangements and genomic disorders. *Trends in genetics : TIG*, **18**, 74-82.
26. Carvalho, C.M. and Lupski, J.R. (2016) Mechanisms underlying structural variant formation in genomic disorders. *Nature reviews. Genetics*, **17**, 224-238.
27. Korsholm, L.M., Gál, Z., Nieto, B., Quevedo, O., Boukoura, S., Lund, C.C. and Larsen, D.H. (2020) Recent advances in the nucleolar responses to DNA double-strand breaks. *Nucleic Acids Res*, **48**, 9449-9461.
28. Warmerdam, D.O., van den Berg, J. and Medema, R.H. (2016) Breaks in the 45S rDNA Lead to Recombination-Mediated Loss of Repeats. *Cell reports*, **14**, 2519-2527.
29. Harding, S.M. and Greenberg, R.A. (2016) Choreographing the Double Strand Break Response: Ubiquitin and SUMO Control of Nuclear Architecture. *Frontiers in genetics*, **7**, 103.
30. van Sluis, M. and McStay, B. (2015) A localized nucleolar DNA damage response facilitates recruitment of the homology-directed repair machinery independent of cell cycle stage. *Genes Dev*, **29**, 1151-1163.
31. Janderova-Rossmeislova, L., Novakova, Z., Vlasakova, J., Philimonenko, V., Hozak, P. and Hodny, Z. (2007) PML protein association with specific nucleolar structures differs in normal, tumor and senescent human cells. *J Struct Biol*, **159**, 56-70.
32. Bernardi, R., Scaglioni, P.P., Bergmann, S., Horn, H.F., Vousden, K.H. and Pandolfi, P.P. (2004) PML regulates p53 stability by sequestering Mdm2 to the nucleolus. *Nat Cell Biol*, **6**, 665-672.
33. Shav-Tal, Y., Blechman, J., Darzacq, X., Montagna, C., Dye, B.T., Patton, J.G., Singer, R.H. and Zipori, D. (2005) Dynamic sorting of nuclear components into distinct nucleolar caps during transcriptional inhibition. *Mol Biol Cell*, **16**, 2395-2413.
34. Condemine, W., Takahashi, Y., Le Bras, M. and de The, H. (2007) A nucleolar targeting signal in PML-I addresses PML to nucleolar caps in stressed or senescent cells. *J Cell Sci*, **120**, 3219-3227.
35. Mattsson, K., Pokrovskaja, K., Kiss, C., Klein, G. and Szekely, L. (2001) Proteins associated with the promyelocytic leukemia gene product (PML)-containing nuclear body move to the nucleolus upon inhibition of proteasome-dependent protein degradation. *Proc Natl Acad Sci U S A*, **98**, 1012-1017.
36. Imrichova, T., Hubackova, S., Kucerova, A., Kosla, J., Bartek, J., Hodny, Z. and Vasicova, P. (2019) Dynamic PML protein nucleolar associations with persistent DNA damage lesions in response to nucleolar stress and senescence-inducing stimuli. *Aging*, **11**, 7206-7235.
37. Hornofova, T., Pokorna, B., Hubackova, S.S., Uvizl, A., Kosla, J., Bartek, J., Hodny, Z. and Vasicova, P. (2022) Phospho-SIM and exon8b of PML protein regulate formation of doxorubicin-induced rDNA-PML compartment. *DNA Repair*, **114**, 103319.

38. Huang, F., Motlekar, N.A., Burgwin, C.M., Napper, A.D., Diamond, S.L. and Mazin, A.V. (2011) Identification of specific inhibitors of human RAD51 recombinase using high-throughput screening. *ACS chemical biology*, **6**, 628-635.
39. Leahy, J.J., Golding, B.T., Griffin, R.J., Hardcastle, I.R., Richardson, C., Rigoreau, L. and Smith, G.C. (2004) Identification of a highly potent and selective DNA-dependent protein kinase (DNA-PK) inhibitor (NU7441) by screening of chromenone libraries. *Bioorganic & medicinal chemistry letters*, **14**, 6083-6087.
40. Cortes Ledesma, F., El Khamisy, S.F., Zuma, M.C., Osborn, K. and Caldecott, K.W. (2009) A human 5'-tyrosyl DNA phosphodiesterase that repairs topoisomerase-mediated DNA damage. *Nature*, **461**, 674-678.
41. Stoddard, B.L. (2005) Homing endonuclease structure and function. *Quarterly reviews of biophysics*, **38**, 49-95.
42. Berkovich, E., Monnat, R.J., Jr. and Kastan, M.B. (2007) Roles of ATM and NBS1 in chromatin structure modulation and DNA double-strand break repair. *Nat Cell Biol*, **9**, 683-690.
43. Banaszynski, L.A., Chen, L.C., Maynard-Smith, L.A., Ooi, A.G. and Wandless, T.J. (2006) A rapid, reversible, and tunable method to regulate protein function in living cells using synthetic small molecules. *Cell*, **126**, 995-1004.
44. Mais, C., Wright, J.E., Prieto, J.L., Raggett, S.L. and McStay, B. (2005) UBF-binding site arrays form pseudo-NORs and sequester the RNA polymerase I transcription machinery. *Genes Dev*, **19**, 50-64.
45. Chen, H., Liu, X. and Patel, D.J. (1996) DNA bending and unwinding associated with actinomycin D antibiotics bound to partially overlapping sites on DNA. *J Mol Biol*, **258**, 457-479.
46. Wang, J.C. (2002) Cellular roles of DNA topoisomerases: a molecular perspective. *Nat Rev Mol Cell Biol*, **3**, 430-440.
47. Pommier, Y., Nussenzweig, A., Takeda, S. and Austin, C. (2022) Human topoisomerases and their roles in genome stability and organization. *Nat Rev Mol Cell Biol*, **23**, 407-427.
48. Linka, R.M., Porter, A.C., Volkov, A., Mielke, C., Boege, F. and Christensen, M.O. (2007) C-terminal regions of topoisomerase IIalpha and IIbeta determine isoform-specific functioning of the enzymes in vivo. *Nucleic Acids Res*, **35**, 3810-3822.
49. Grue, P., Grässer, A., Sehested, M., Jensen, P.B., Uhse, A., Straub, T., Ness, W. and Boege, F. (1998) Essential mitotic functions of DNA topoisomerase IIalpha are not adopted by topoisomerase IIbeta in human H69 cells. *J Biol Chem*, **273**, 33660-33666.
50. Lee, J.H. and Berger, J.M. (2019) Cell Cycle-Dependent Control and Roles of DNA Topoisomerase II. *Genes*, **10**, 18.
51. Daniloski, Z., Bisht, K.K., McStay, B. and Smith, S. (2019) Resolution of human ribosomal DNA occurs in anaphase, dependent on tankyrase 1, condensin II, and topoisomerase IIalpha. *Genes Dev*, **33**, 276-281.
52. Wu, H.Y., Shyy, S.H., Wang, J.C. and Liu, L.F. (1988) Transcription generates positively and negatively supercoiled domains in the template. *Cell*, **53**, 433-440.
53. Marchand, C., Pourquier, P., Laco, G.S., Jing, N. and Pommier, Y. (2002) Interaction of human nuclear topoisomerase I with guanosine quartet-forming and guanosine-rich single-stranded DNA and RNA oligonucleotides. *J Biol Chem*, **277**, 8906-8911.
54. French, S.L., Sikes, M.L., Hontz, R.D., Osheim, Y.N., Lambert, T.E., El Hage, A., Smith, M.M., Tollervey, D., Smith, J.S. and Beyer, A.L. (2011) Distinguishing the roles of Topoisomerases I and II in relief of transcription-induced torsional stress in yeast rRNA genes. *Mol Cell Biol*, **31**, 482-494.
55. Saha, S. and Pommier, Y. (2023) R-loops, type I topoisomerases and cancer. *NAR Cancer*, **5**.
56. Willmore, E., Frank, A.J., Padget, K., Tilby, M.J. and Austin, C.A. (1998) Etoposide targets topoisomerase IIalpha and IIbeta in leukemic cells: isoform-specific cleavable complexes

visualized and quantified in situ by a novel immunofluorescence technique. *Molecular pharmacology*, **54**, 78-85.

57. Atwal, M., Swan, R.L., Rowe, C., Lee, K.C., Lee, D.C., Armstrong, L., Cowell, I.G. and Austin, C.A. (2019) Intercalating TOP2 Poisons Attenuate Topoisomerase Action at Higher Concentrations. *Molecular pharmacology*, **96**, 475-484.
58. Frank, N.E., Cusack, B.J., Talley, T.T., Walsh, G.M. and Olson, R.D. (2016) Comparative effects of doxorubicin and a doxorubicin analog, 13-deoxy, 5-iminodoxorubicin (GPX-150), on human topoisomerase IIβ activity and cardiac function in a chronic rabbit model. *Investigational new drugs*, **34**, 693-700.
59. Hasinoff, B.B., Wu, X., Patel, D., Kanagasabai, R., Karmahapatra, S. and Yalowich, J.C. (2016) Mechanisms of Action and Reduced Cardiotoxicity of Pixantrone; a Topoisomerase II Targeting Agent with Cellular Selectivity for the Topoisomerase IIα Isoform. *The Journal of pharmacology and experimental therapeutics*, **356**, 397-409.
60. Pang, B., Qiao, X., Janssen, L., Velds, A., Groothuis, T., Kerkhoven, R., Nieuwland, M., Ovaa, H., Rottenberg, S., van Tellingen, O. *et al.* (2013) Drug-induced histone eviction from open chromatin contributes to the chemotherapeutic effects of doxorubicin. *Nat Commun*, **4**, 1908.
61. Berlin, V. and Haseltine, W.A. (1981) Reduction of adriamycin to a semiquinone-free radical by NADPH cytochrome P-450 reductase produces DNA cleavage in a reaction mediated by molecular oxygen. *J Biol Chem*, **256**, 4747-4756.
62. Gajewski, E., Gaur, S., Akman, S.A., Matsumoto, L., van Balgooy, J.N. and Doroshow, J.H. (2007) Oxidative DNA base damage in MCF-10A breast epithelial cells at clinically achievable concentrations of doxorubicin. *Biochem Pharmacol*, **73**, 1947-1956.
63. Canela, A., Maman, Y., Huang, S.N., Wutz, G., Tang, W., Zagnoli-Vieira, G., Callen, E., Wong, N., Day, A., Peters, J.M. *et al.* (2019) Topoisomerase II-Induced Chromosome Breakage and Translocation Is Determined by Chromosome Architecture and Transcriptional Activity. *Mol Cell*, **75**, 252-266 e258.
64. Zeng, Z., Cortés-Ledesma, F., El Khamisy, S.F. and Caldecott, K.W. (2011) TDP2/TTRAP is the major 5'-tyrosyl DNA phosphodiesterase activity in vertebrate cells and is critical for cellular resistance to topoisomerase II-induced DNA damage. *J Biol Chem*, **286**, 403-409.
65. Gómez-Herreros, F., Romero-Granados, R., Zeng, Z., Alvarez-Quilón, A., Quintero, C., Ju, L., Umans, L., Vermeire, L., Huylebroeck, D., Caldecott, K.W. *et al.* (2013) TDP2-dependent non-homologous end-joining protects against topoisomerase II-induced DNA breaks and genome instability in cells and in vivo. *PLoS genetics*, **9**, e1003226.
66. Monnat, R.J., Jr., Hackmann, A.F. and Cantrell, M.A. (1999) Generation of highly site-specific DNA double-strand breaks in human cells by the homing endonucleases I-PpoI and I-CreI. *Biochem Biophys Res Commun*, **255**, 88-93.
67. Maede, Y., Shimizu, H., Fukushima, T., Kogame, T., Nakamura, T., Miki, T., Takeda, S., Pommier, Y. and Murai, J. (2014) Differential and common DNA repair pathways for topoisomerase I- and II-targeted drugs in a genetic DT40 repair cell screen panel. *Mol Cancer Ther*, **13**, 214-220.
68. Schürmann, L., Schumacher, L., Roquette, K., Brozovic, A. and Fritz, G. (2021) Inhibition of the DSB repair protein RAD51 potentiates the cytotoxic efficacy of doxorubicin via promoting apoptosis-related death pathways. *Cancer Lett*, **520**, 361-373.
69. Alagpulinsa, D.A., Ayyadevara, S. and Shmookler Reis, R.J. (2014) A Small-Molecule Inhibitor of RAD51 Reduces Homologous Recombination and Sensitizes Multiple Myeloma Cells to Doxorubicin. *Front Oncol*, **4**, 289.
70. Patra, U. and Müller, S. (2021) A Tale of Usurpation and Subversion: SUMO-Dependent Integrity of Promyelocytic Leukemia Nuclear Bodies at the Crossroad of Infection and Immunity. *Frontiers in cell and developmental biology*, **9**, 696234.

71. Reichelt, M., Wang, L., Sommer, M., Perrino, J., Nour, A.M., Sen, N., Baiker, A., Zerboni, L. and Arvin, A.M. (2011) Entrapment of viral capsids in nuclear PML cages is an intrinsic antiviral host defense against varicella-zoster virus. *PLoS Pathog*, **7**, e1001266.
72. Scherer, M., Read, C., Neusser, G., Kranz, C., Kuderna, A.K., Müller, R., Full, F., Wörz, S., Reichel, A., Schilling, E.M. *et al.* (2022) Dual signaling via interferon and DNA damage response elicits entrapment by giant PML nuclear bodies. *eLife*, **11**, 28.
73. Warmerdam, D.O. and Wolthuis, R.M.F. (2019) Keeping ribosomal DNA intact: a repeating challenge. *Chromosome research : an international journal on the molecular, supramolecular and evolutionary aspects of chromosome biology*, **27**, 57-72.
74. Rueden, C.T., Schindelin, J., Hiner, M.C., DeZonia, B.E., Walter, A.E., Arena, E.T. and Eliceiri, K.W. (2017) ImageJ2: ImageJ for the next generation of scientific image data. *BMC bioinformatics*, **18**, 529.
75. Schindelin, J., Arganda-Carreras, I., Frise, E., Kaynig, V., Longair, M., Pietzsch, T., Preibisch, S., Rueden, C., Saalfeld, S., Schmid, B. *et al.* (2012) Fiji: an open-source platform for biological-image analysis. *Nature methods*, **9**, 676-682.
76. Rizk, A., Paul, G., Incardona, P., Bugarski, M., Mansouri, M., Niemann, A., Ziegler, U., Berger, P. and Sbalzarini, I.F. (2014) Segmentation and quantification of subcellular structures in fluorescence microscopy images using Squassh. *Nature protocols*, **9**, 586-596.

Figure legends

Figure 1. PNAs formation after diverse stress-inducing stimuli and topoisomerase downregulation. (**A**) Structural types of PML nucleolar associations (PNAs) – 'bowls', 'funnels', 'balloons', and PML nucleolus-derived structures (PML-NDS) occurring in RPE-1^{hTERT} cells after treatment with 0.75 μM doxorubicin detected by indirect immunofluorescence with anti-PML antibody (green) and counter-stained with TOTO-3 (red, for nucleoli visualization) and DAPI (blue). Scale bar, 10 μm. (**B**) Quantification of the percentage of RPE-1^{hTERT} cells containing PNAs, 48 hours after treatment with various stress-inducing stimuli. The stress stimuli were divided into five categories according to their mechanism of action: 1) inhibitors of topoisomerases, 2) inhibitors of RNAP I, 3) inhibitors of pre-RNA processing, 4) inductors of replication stress, and 5) other stressors. p53 stabilization, γH2AX foci formation, PAF49 segregation, and TOP1 or TOP2a decline have been assessed for each treatment. (**C**) The pattern of PML (green) and B23 (red) in RPE-1^{hTERT} cells, visualized by indirect immunofluorescence, after transfection with esiRNAs targeting topoisomerases 1 and 2alpha, with siRNA targeting topoisomerase 2beta, or with non-targeting siRNA, respectively. Scale bar, 10 μm. (**D**) RPE-1^{hTERT} cells were pre-treated with 10 nM AMD for 5 hours or with 5 μM CX-5461 for 2 hours to inhibit RNAPI. The cells were then treated with 0.375 μM or 0.75 μM doxorubicin or transfected with esiRNA targeting TOP1 for 48 hours. The bar graphs show the percentage of cells containing either PML-NDS or bowls/funnels/balloons for three independent experiments (graph 1), for a single experiment (graph 2), or for three biological replicates (graph 3). Results are presented as a mean ± s.d.

Figure 2. Inhibition of DNA repair augmented the PNAs formation. RPE-1^{hTERT} cells were treated with doxorubicin and three concentrations of B02 or with etoposide after downregulation of TDP2 by RNA interference. After the treatment, the PML (green) and nucleolar marker B23 (red) were visualized by indirect immunofluorescence and wide-field fluorescent microscopy, and a number of nuclei with PNAS were analyzed. (**A**) The bar graph represents the percentage of nuclei with PNAs after 2-day-long treatment with doxorubicin (0.375 µM or 0.56 µM), three concentrations of B02 (5, 10, and 20 µM), and corresponding concentrations of DMSO as a mock. (**B**) The bar graph represents the distribution of individual types of PNAs after the same treatments as in shown in (A). (**C**) Representative cells after 2-day-long treatment with 0.375 µM doxorubicin combined with 20 µM B02 or 0.1% DMSO (mock). (**D**) Representative cells after 2-day-long treatment with 0.56 µM doxorubicin combined with 20 µM B02 or 0.1% DMSO (mock). (**E**) The bar graph represents the percentage of nuclei with PNAs after 4 days of recovery from 2-day-long treatments with doxorubicin (0.375 µM or 0.56 µM) together with three concentrations of B02 (5, 10, and 20 µM), and corresponding concentrations of DMSO. (**F**) Representative cells after 4 days of recovery from 2-day-long treatment with 0.375 µM doxorubicin combined with 20 µM B02 or 0.1% DMSO (mock). (**G**) Representative cells after 4 days of recovery from 2-day-long treatment with 0.56 µM doxorubicin combined with 20 µM B02 or 0.1% DMSO (mock). (**H**) The bar graph represents the percentage of nuclei with PNAs after 2-day-long treatment with 5 µM etoposide in cells where TDP2 was downregulated by RNA interference. In all experiments, at least three biological replicates were evaluated. Results are presented as a mean ± s.d. Student's t-test was used for statistical evaluation. Asterisks indicate the following: ****P < 0.0001, ***P < 0.001, **P < 0.01, *P < 0.05. Scale bar, 20 µm.

Figure 3. PNAs encircle rDNA and DJ loci containing DNA DSB after doxorubicin treatment. RPE-1^{hTERT} cells were treated with 0.75 µM doxorubicin for 2 days and recovered from the treatment for one and four days. The proliferating cells were used as a control. The localization of rDNA, DJ, PML, and 53BP1 was analyzed using immuno-FISH staining and confocal microscopy. (**A**) The scheme of a human acrocentric chromosome. The position of probes used for the detection of the rDNA locus (blue) and DJ locus (grey) is shown. (**B**) The representative nuclei and the nucleoli with and without PNAs in control and treated cells are shown. rDNA (red), DJ (white), PML (green), and 53BP1 (red). (**C**) The extent of PML-rDNA and PML-DJ size-based colocalization calculated for individual nucleoli of treated and untreated cells with respect to the presence of PNAs is shown as a scatter plot. The median with an interquartile range is shown. The colocalization was calculated using Fiji(ImageJ)/ Mosaic/Segmentation/Squassh plugin. The number of analyzed nucleoli in each group was: ctrl (n=26); 2 days + PNAs (n=28); 2 days without PNAs (n=18); 1-day-long recovery + PNAs (n=38); 1-day-long recovery without PNAs (n=20); 4-day-long recovery + PNAs (n=23); 4-day-long recovery without PNAs (n=24). (**D**) The extent of 53BP1-rDNA and 53BP1-DJ size-based

colocalization calculated for individual nucleoli of treated and untreated cells with respect to the presence of PNAs is shown as a scatter plot. The median with interquartile range is shown. The same collection of nucleoli was used as presented in (C). (**E**) The example of analysis that was used to identify whether rDNA/DJ with DNA DSB colocalized with PNAs. The images of the representative nucleoli (2 days doxorubicin, 1- and 4-days recovery) after deconvolution, segmentation, and its 3D model are shown. Note, that the signal of all observed markers was identified as a unique 3D object. rDNA (blue), DJ (white), PML (green), and 53BP1 (red). (**F**) The combined bar graph shows the percentage of PNAs containing rDNA/DJ with DNA DSB, rDNA/DJ without DNA DSB, and PNAs in which the rDNA/DJ signal was not detected. The number of analyzed nucleoli: 2 days doxorubicin (n=28), 1-day-long recovery (n=39), 4-day-long recovery (n=21). Student's t-test was used for statistical evaluation. Asterisks indicate the following: ****P < 0.0001, ***P < 0.001, **P < 0.01, *P < 0.05. Scale bars, 10 μm (nuclei in B and E) and 5 μm (nucleoli in B).

Figure 4. The DNA damage introduced into the rDNA locus by endonuclease I-PpoI induces PML-NDS. (**A**) Scheme of inducible expression of endonuclease I-PpoI in RPE-1^{hTERT} cells and the position of I-PpoI cleavage site in rDNA locus. (**B**) Scheme of the experimental setup used in all experiments presented. Briefly, I-PpoI was activated by doxycycline and Shield for 24 hours, then the medium was exchanged, and the cells were analyzed upon the recovery phase (0, 1, 2, and 5 days). (**C**) The representative images obtained by indirect immunofluorescence and confocal microscopy (Stellaris) show the localization of 53BP1 (a marker of DNA DSB, red), and PML (green) upon 1-day-long activation of I-PpoI and during recovery from I-PpoI insult. The nucleus and nucleolus were marked by DAPI (blue), and TOTO-3 (white), respectively. Only one layer from the several sections is presented. (**D**) The level of DNA DSB upon the recovery from I-PpoI insult was obtained by detecting the 53BP1 (a marker of DNA DSB) by indirect immunofluorescence and high-content microscopy unit (ScanR). The histogram represents the frequency of nuclei (%) with the same number of 53BP1 foci. The bin center used for analysis was 2. (**E**) The number of nuclei with PNAs upon the recovery from I-PpoI insult was obtained by detection of PML using indirect immunofluorescence and a high-content microscopy unit (ScanR). The quantification was done manually by the evaluation of PML localization in more than 200 nuclei. The bar graph represents the percentage of nuclei with PNAs. Results are presented as a mean ± s.d. obtained from three biological replicates. (**F**) The representative images obtained by indirect immunofluorescence and confocal microscopy (Stellaris) show the correlation between the localization of B23 (red) in PML-NDS (PML, green) upon the recovery from I-PpoI insult. The nucleus and nucleolus were marked by DAPI (blue), and TOTO-3 (white), respectively. Only one layer from the several sections is presented. (**G**) The representative images obtained by indirect immunofluorescence and wide-field microscopy show the correlation between the localization of DHX9 (red) and PML-NDS (PML, green) upon the recovery from I-PpoI insult. The nucleus and nucleolus were marked by DAPI (blue), and TOTO-3 (white), respectively.

(**H-I**) The representative images obtained by indirect immunofluorescence and confocal microscopy (Stellaris) show the localization of UBF ((H), a marker of rDNA; red) or PAF49((I), a subunit of RNAPI; red) in PML-NDS (PML, green) upon the recovery from I-PpoI insult. One layer of the nucleus and three sequential layers of nucleolus with PML-NDS are presented. The nucleus and nucleolus were marked by DAPI (blue) and by TOTO-3 (white), respectively. Scale bars, 10 µm (nuclei C, F, G, H, and I) and 5 µm (nucleoli H and I).

Figure 5. Inhibition of RAD51/homologous recombination suppressed the formation of I-PpoI-induced PML-NDS. (**A**) Scheme of the experimental setup used in all experiments presented in this figure. Briefly, I-PpoI was activated in RPE-1hTERT-I-PpoI cell clones 1A11 and 1H4 by doxycycline and Shield for 24 hours. The inhibitors of DNA PK (1 µM Nu7441) or RAD51 (10 µM B02) were applied individually or both together. After the 24-hour long activation, the medium was exchanged and the cells were analyzed during the recovery phase (0, 1, 2, and 5 days). (**B** and **C**) During the recovery phase the level of DNA DSB was quantified by the detection of 53BP1 (a marker DNA DSB) using indirect immunofluorescence and a high-content microscopy unit (ScanR). The data from three independent biological replicates were pooled together and represented as the Whiskers box (10 – 90 percentile) or as the histograms showing the frequency of nuclei (%) with the same number of 53BP1 foci. The bin center used for analysis was 2. Clones 1A11 and 1H4 are shown in (B) and (C), respectively. (**D** and **E**) The number of nuclei with PNAs upon the recovery from I-PpoI insult and simultaneous inhibition of particular DNA damage repair pathway was obtained by detection of PML using indirect immunofluorescence and a high-content microscopy unit (ScanR). The quantification was done manually by the evaluation of PML localization in more than 200 nuclei. The bar plot represents the fold-change of the percentage of nuclei with PNAs relatively to mock. Results are presented as a mean ± s.d. obtained from three biological replicates. Asterisks indicate the following: ****$P < 0.0001$, ***$P < 0.001$, **$P < 0.01$, *$P < 0.05$.

Figure 1

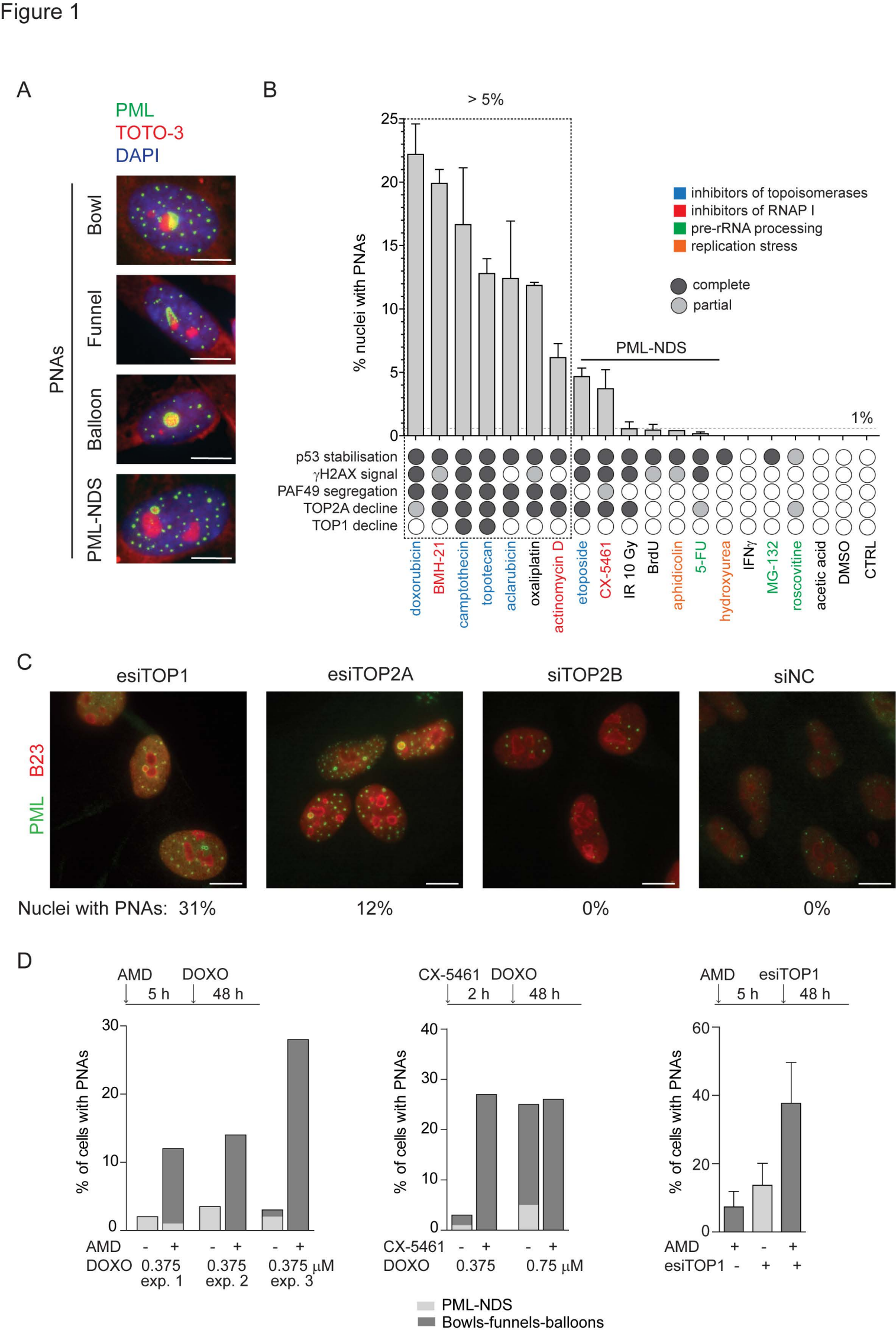
A
PML
TOTO-3
DAPI
PNAs
Bowl
Funnel
Balloon
PML-NDS
B
> 5%
% nuclei with PNAs
inhibitors of topoisomerases
inhibitors of RNAP I
pre-rRNA processing
replication stress
complete
partial
PML-NDS
1%
p53 stabilisation
γH2AX signal
PAF49 segregation
TOP2A decline
TOP1 decline
doxorubicin
BMH-21
camptothecin
topotecan
aclarubicin
oxaliplatin
actinomycin D
etoposide
CX-5461
IR 10 Gy
BrdU
aphidicolin
5-FU
hydroxyurea
IFNγ
MG-132
roscovitine
acetic acid
DMSO
CTRL
C
esiTOP1
esiTOP2A
siTOP2B
siNC
PML
B23
Nuclei with PNAs: 31%
12%
0%
0%
D
AMD
DOXO
5 h
48 h
% of cells with PNAs
AMD
DOXO
0.375
0.375
0.375 μM
exp. 1
exp. 2
exp. 3
CX-5461
DOXO
2 h
48 h
CX-5461
DOXO
0.375
0.75 μM
AMD
esiTOP1
5 h
48 h
AMD
esiTOP1
PML-NDS
Bowls-funnels-balloons

Figure 2

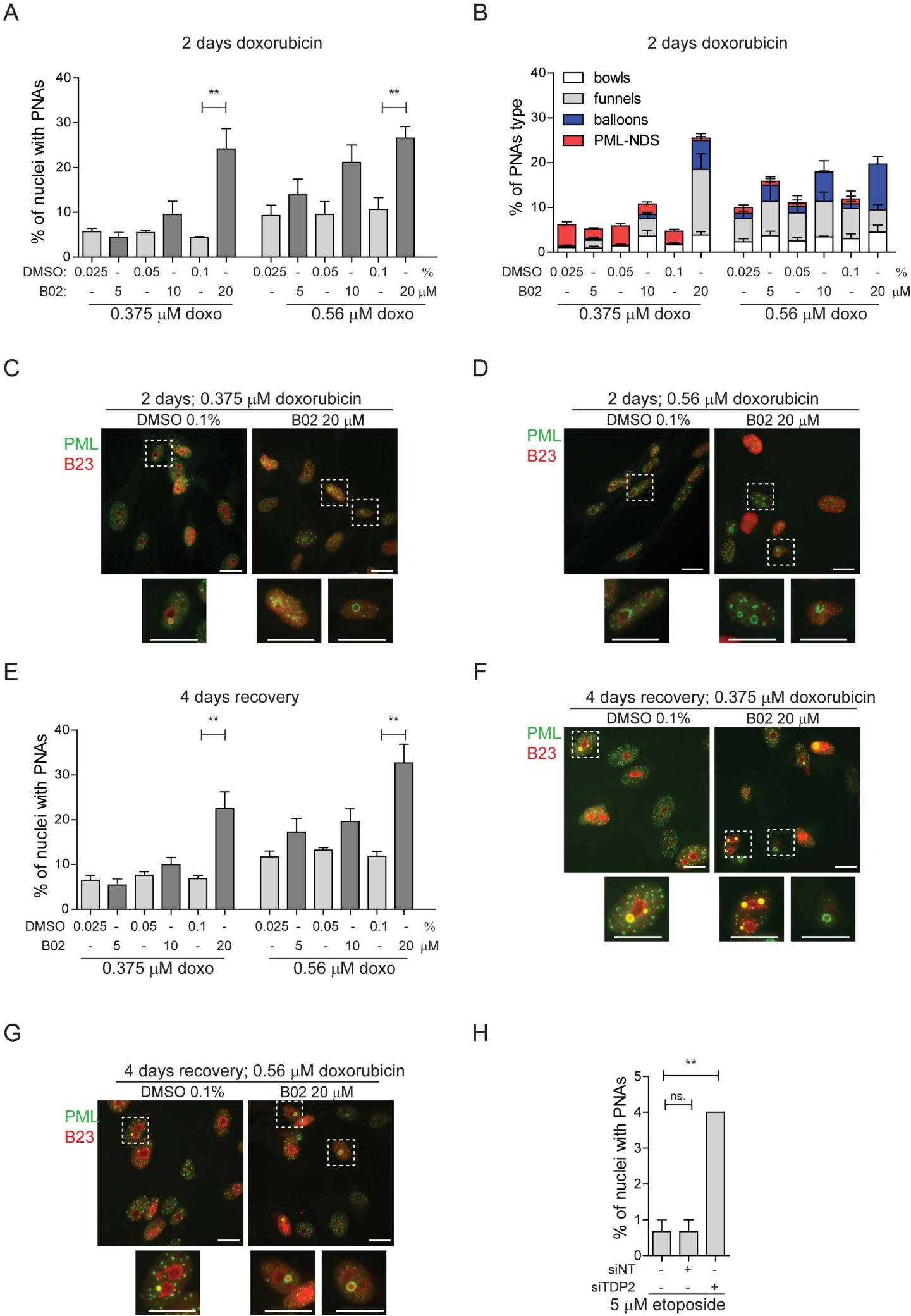
A
2 days doxorubicin
% of nuclei with PNAs
DMSO: 0.025 - 0.05 - 0.1 - 0.025 - 0.05 - 0.1 - %
B02: - 5 - 10 - 20 - 5 - 10 - 20 μM
0.375 μM doxo
0.56 μM doxo
B
2 days doxorubicin
% of PNAs type
bowls
funnels
balloons
PML-NDS
DMSO 0.025 - 0.05 - 0.1 - 0.025 - 0.05 - 0.1 - %
B02 - 5 - 10 - 20 - 5 - 10 - 20 μM
0.375 μM doxo
0.56 μM doxo
C
2 days; 0.375 μM doxorubicin
DMSO 0.1%
B02 20 μM
PML
B23
D
2 days; 0.56 μM doxorubicin
DMSO 0.1%
B02 20 μM
PML
B23
E
4 days recovery
% of nuclei with PNAs
DMSO 0.025 - 0.05 - 0.1 - 0.025 - 0.05 - 0.1 - %
B02 - 5 - 10 - 20 - 5 - 10 - 20 μM
0.375 μM doxo
0.56 μM doxo
F
4 days recovery; 0.375 μM doxorubicin
DMSO 0.1%
B02 20 μM
PML
B23
G
4 days recovery; 0.56 μM doxorubicin
DMSO 0.1%
B02 20 μM
PML
B23
H
% of nuclei with PNAs
ns.
siNT - + -
siTDP2 - - +
5 μM etoposide

Figure 3

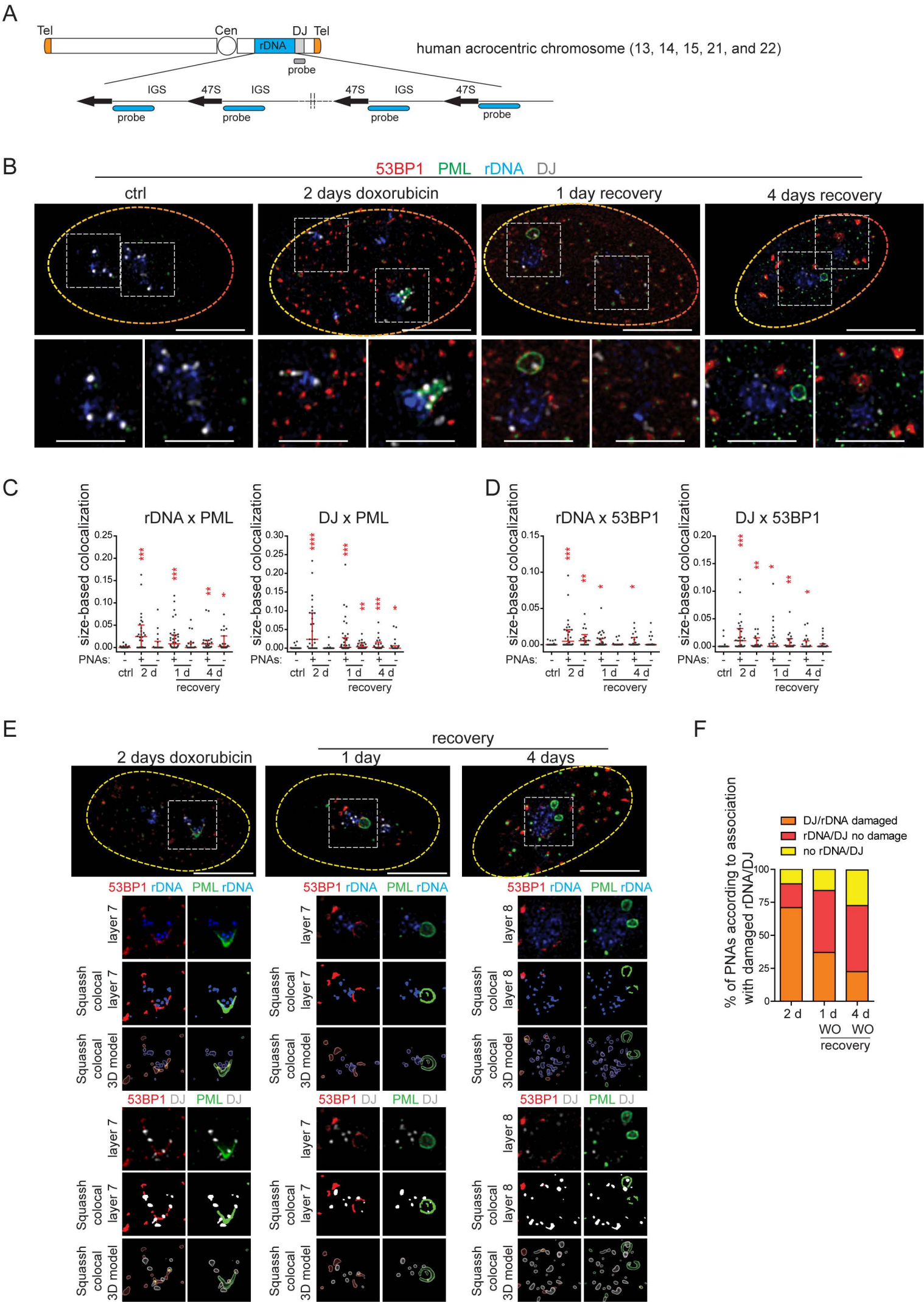
A
Tel
Cen
DJ
Tel
rDNA
probe
human acrocentric chromosome (13, 14, 15, 21, and 22)
IGS
47S
IGS
47S
IGS
47S
probe
probe
probe
probe
B
53BP1 PML rDNA DJ
ctrl
2 days doxorubicin
1 day recovery
4 days recovery
C
rDNA x PML
DJ x PML
size-based colocalization
PNAs:
ctrl
2 d
1 d
4 d
recovery
D
rDNA x 53BP1
DJ x 53BP1
size-based colocalization
PNAs:
ctrl
2 d
1 d
4 d
recovery
E
2 days doxorubicin
recovery
1 day
4 days
53BP1 rDNA PML rDNA
53BP1 DJ PML DJ
layer 7
layer 8
Squassh colocal layer 7
Squassh colocal layer 8
Squassh colocal 3D model
F
DJ/rDNA damaged
rDNA/DJ no damage
no rDNA/DJ
% of PNAs according to association with damaged rDNA/DJ
2 d
1 d WO
4 d WO
recovery

Figure 4

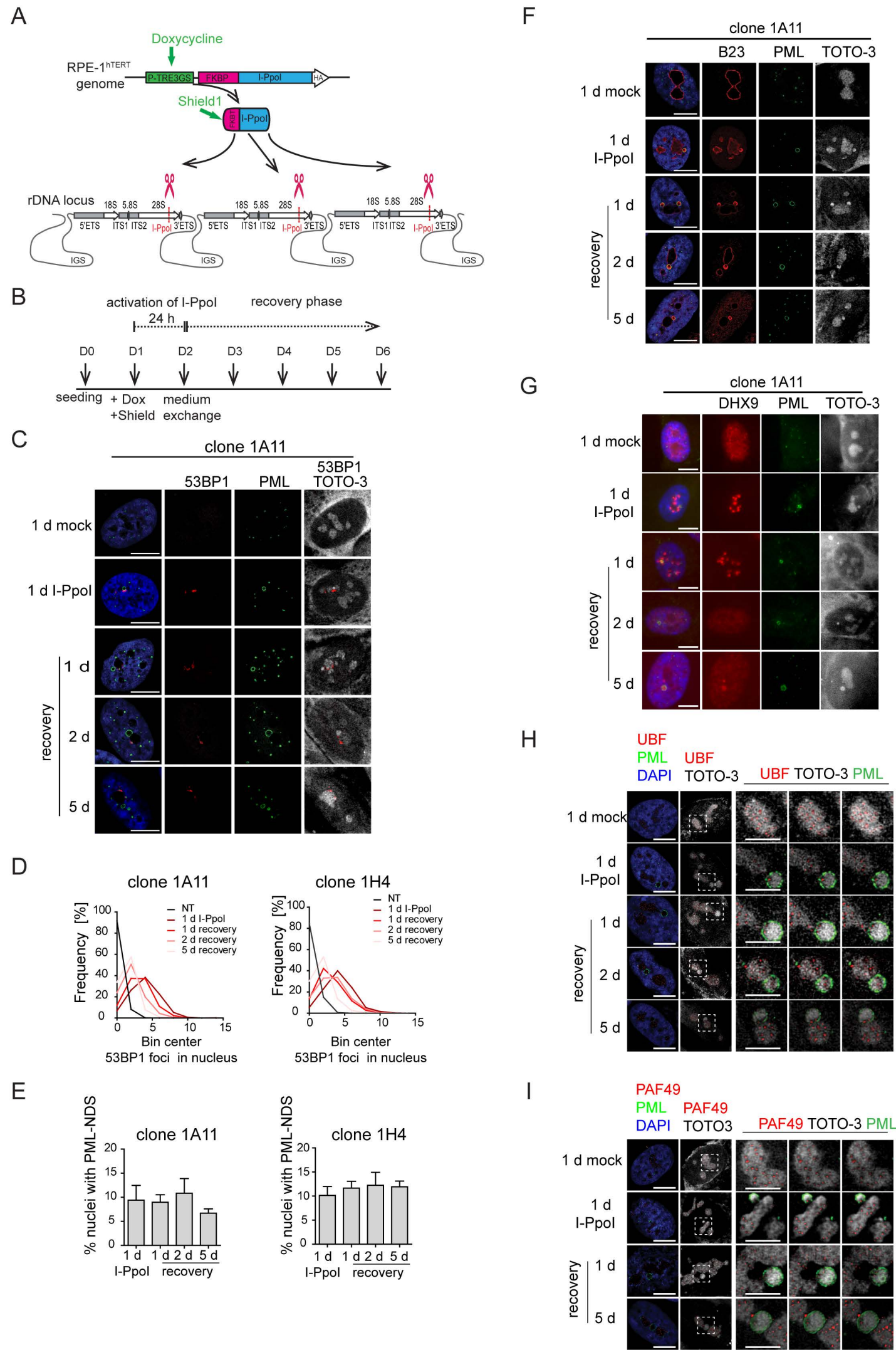
A
Doxycycline
RPE-1hTERT genome
P-TRE3GS
FKBP
I-PpoI
HA
Shield1
rDNA locus
18S 5.8S 28S
5'ETS ITS1 ITS2 I-PpoI 3'ETS
IGS
B
activation of I-PpoI
24 h
recovery phase
D0 D1 D2 D3 D4 D5 D6
seeding
+ Dox +Shield
medium exchange
C
clone 1A11
53BP1
PML
53BP1 TOTO-3
1 d mock
1 d I-PpoI
recovery
1 d
2 d
5 d
D
clone 1A11
clone 1H4
Frequency [%]
NT
1 d I-PpoI
1 d recovery
2 d recovery
5 d recovery
Bin center
53BP1 foci in nucleus
E
clone 1A11
clone 1H4
% nuclei with PML-NDS
1 d 1 d 2 d 5 d
I-PpoI recovery
F
clone 1A11
B23
PML
TOTO-3
1 d mock
1 d I-PpoI
recovery
1 d
2 d
5 d
G
clone 1A11
DHX9
PML
TOTO-3
1 d mock
1 d I-PpoI
recovery
1 d
2 d
5 d
H
UBF
PML
DAPI
UBF TOTO-3
UBF TOTO-3 PML
1 d mock
1 d I-PpoI
recovery
1 d
2 d
5 d
I
PAF49
PML
DAPI
PAF49 TOTO3
PAF49 TOTO-3 PML
1 d mock
1 d I-PpoI
recovery
1 d
5 d

Figure 5

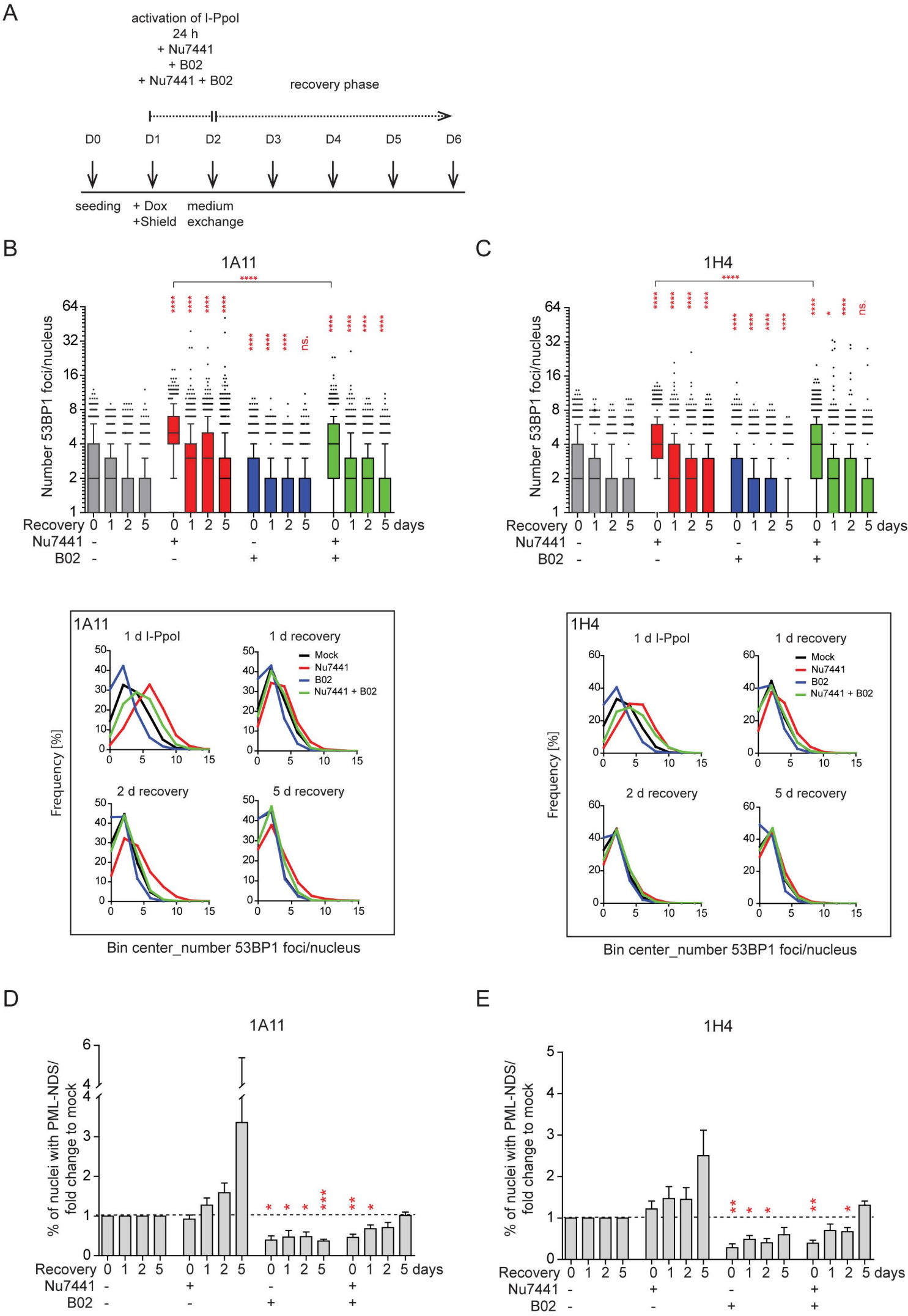
A
activation of I-PpoI
24 h
+ Nu7441
+ B02
+ Nu7441 + B02
recovery phase
D0
D1
D2
D3
D4
D5
D6
seeding
+ Dox
+Shield
medium
exchange
B
1A11
Number 53BP1 foci/nucleus
Recovery 0 1 2 5 0 1 2 5 0 1 2 5 0 1 2 5 days
Nu7441 - + - +
B02 - - + +
C
1H4
Number 53BP1 foci/nucleus
Recovery 0 1 2 5 0 1 2 5 0 1 2 5 0 1 2 5 days
Nu7441 - + - +
B02 - - + +
1A11
1 d I-PpoI
1 d recovery
2 d recovery
5 d recovery
Mock
Nu7441
B02
Nu7441 + B02
Frequency [%]
Bin center_number 53BP1 foci/nucleus
1H4
1 d I-PpoI
1 d recovery
2 d recovery
5 d recovery
Mock
Nu7441
B02
Nu7441 + B02
Frequency [%]
Bin center_number 53BP1 foci/nucleus
D
1A11
% of nuclei with PML-NDS/
fold change to mock
Recovery 0 1 2 5 0 1 2 5 0 1 2 5 0 1 2 5 days
Nu7441 - + - +
B02 - - + +
E
1H4
% of nuclei with PML-NDS/
fold change to mock
Recovery 0 1 2 5 0 1 2 5 0 1 2 5 0 1 2 5 days
Nu7441 - + - +
B02 - - + +